Bone Reports 30 (2026) 101937

Contents lists available at ScienceDirect

Bone Reports

journal homepage: www.elsevier.com/locate/bonr

Sost deficiency leads to greater bone vascular porosity, but similar osteocyte lacunar properties with increasing age

Taylor deVet [a,b], Anthony Helou [b], Sara Checa [c], Alexander Rack [d], Ina Kramer [e], Fabian Wilde [f], Paul Zaslansky [g], Bettina M. Willie [a,b,h,i,*]

[a] *Department of Biomedical Engineering, McGill University, Montreal, Canada*
[b] *Research Centre, Shriners Hospitals for Children, Montreal, Canada*
[c] *Institute of Biomechanics, Hamburg University of Technology, Hamburg, Germany*
[d] *ESRF - The European Synchrotron, Grenoble, France*
[e] *Novartis Biomedical Research, Basel, Switzerland*
[f] *Helmholtz-Zentrum Geesthacht, 21502, Geesthacht, Germany*
[g] *Department for Operative, Preventive and Pediatric Dentistry, Charité-Universitätsmedizin, Berlin, Germany*
[h] *College of Veterinary Medicine, Utah State University, Logan, UT, USA*
[i] *Julius Wolff Institute, Charité-Universitätsmedizin Berlin, Berlin, Germany*

ARTICLE INFO

Keywords:
Fracture healing
Aging
Sost knockout
Synchrotron tomography
Sclerostin neutralizing antibody
Bone vascular porosity
Lacunar properties

ABSTRACT

Sclerostin neutralizing antibody is an approved anabolic drug used to increase bone mass. Numerous preclinical studies examined bone mass and microstructural changes in mice receiving sclerostin neutralizing antibodies or mice lacking sclerostin, such as *Sost* knock out mice. Surprisingly no preclinical studies examined the effect of sclerostin deficiency with aging, despite the treatment being used primarily in older individuals. Thus, our primary aim was to examine the effect of long-term *Sost* deficiency on bone microstructure, including osteocyte lacunar and bone vascular porosity properties across ages. Our results show that *Sost* deletion led to sustained bone formation across the mouse's lifespan, whereas wild-type control mice experienced bone maturation followed by age-related declines in bone volume. Lacunar parameters were also affected due to *Sost* deletion, with altered lacunar density and volume in young mice, but these differences were not present in old mice. Our secondary aim was to examine the effect of short-term sclerostin deficiency on bone microporosity in woven and cortical bone after an osteotomy in adult female C57BL6J mice. Short term sclerostin antibody treatment did not alter vascular or lacunar porosity within lamellar or newly formed woven bone, suggesting that timing and duration are critical for therapeutic efficacy. In summary, *Sost* KO mice exhibit sustained cortical thickening and pronounced bone vascular porosity, particularly as the mice aged. As sclerostin neutralizing antibody becomes more widely used in an aging population, for extended periods of time, this work helps us understand the effects of long-term inhibition.

1. Introduction

Wnt signaling is a major molecular pathway regulating bone formation. Sclerostin, a Wnt signaling inhibitor, is a small protein produced primarily by osteocytes that is encoded by the *SOST* gene (Brunkow et al., 2001). Sclerostin inhibits the canonical Wnt signaling pathway through binding to LRP5 and 6, thereby suppressing osteoblast differentiation and bone formation and increasing osteocyte/osteoblast RANKL-mediated osteoclastogenesis and bone resorption (Kogawa et al., 2013; Wijenayaka et al., 2011). Loss of sclerostin causes high bone mass disorders (sclerosteosis and van Buchem disease), while overexpression results in low bone mass (Burr and Allen, 2019). Sclerostin neutralizing antibody therapy has been approved for the treatment of postmenopausal osteoporosis (Mcclung et al., 2014) and for clinical use in men with severe osteoporosis (Lewiecki et al., 2018). Clinical trials are also ongoing for treatment of osteogenesis imperfecta in adults and children (Glorieux et al., 2017, 2024; Hosseinitabatabaei et al., 2025; Rummler et al., 2024). Previously, sclerostin neutralizing antibody therapy was tested for treatment of tibial diaphyseal fractures (Bhandari et al., 2020) and hip fractures (Schemitsch et al., 2020), but both trials

* Corresponding author at: Utah State University, College of Veterinary Medicine, Veterinary Medical Education Bldg., 1185E 1400N, Logan, UT, 84341, USA.
E-mail address: bettina.willie@usu.edu (B.M. Willie).

https://doi.org/10.1016/j.bonr.2026.101937
Received 29 May 2026; Received in revised form 30 June 2026; Accepted 3 July 2026
Available online 6 July 2026

failed to show improved healing outcomes.

In support of the clinical approval of sclerostin neutralizing antibody, a large number of preclinical studies have been conducted. These investigations reported enhanced bone mass and microstructural changes in *Sost* KO mice or mice receiving sclerostin neutralizing antibodies, but surprisingly none examined the effects on aging or included elderly mice. In fact, the oldest mice in which bone mass and microstructure were reported were rather young, only 26 week old male and female *Sost* KO mice (Albiol et al., 2020; Li et al., 2008), though we know of one report examining increased subchondral bone related to osteoarthritis in 16 month old male *Sost* KO mice (Roudier et al., 2013). This is particularly surprising considering that the use of this drug is primarily in older populations with the notable exception of rare bone diseases.

In addition to a lack of data reported on age-related changes in bone mass and microstructure with *Sost* inhibition, there is also a paucity of data on microporosity (lacunae, canaliculi, and vascular canals) changes with *Sost* deficiency. Microporosity is critically important for bone strength and toughness, since pores can act as stress concentrators, depending on their size and orientation with respect to the applied load (Currey, 1988; Muñoz et al., 2025b; Schaffler and Burr, 1988; Wagermaier et al., 2015). The effect on osteocyte lacunar properties is of particular interest because osteocytes are the most abundant cell type within bone, residing in fluid filled lacunae, and are thought to be the main mechanoreceptive cells (Muñoz et al., 2025a). Only one study to date has examined lacunar porosity during *Sost* deficiency, in young (12 week old) male *Sost* KO mice (Mosey et al., 2017). These authors showed that *Sost* KO mice did not have altered lacunar density, with similar lacunar shapes compared to WT mice. Thi was reported at the tibiofibular junction (Mosey et al., 2017), and their evaluation was limited to lacunar size while shape and orientation were not addressed. They also reported no change in vascular canal density in these young male *Sost* KO mice (Mosey et al., 2017). Thus, further investigation of lacunar orientation, size, shape, and number density in cortical bone generated during long or short-term sclerostin deficiency in young as well as adult and elderly mice is warranted.

The effect of sclerostin deficiency on bone vascular pore properties is also of interest due to early reports in human clinical trials that sclerostin inhibition led to increased cardiovascular events (Lewiecki et al., 2018; Saag et al., 2017). A recent meta-analysis indicated a sclerostin neutralizing antibody could result in thicker carotid intima media, arterial calcification, but up to the present time there has been no reports of increased risk of major adverse cardiovascular events in clinical studies (Catalano et al., 2020; De Maré et al., 2022; Dreyer et al., 2023; Golledge and Thanigaimani, 2022; Langdahl et al., 2021). However, sclerostin is very important for angiogenesis-osteogenesis coupling (Oranger et al., 2017). We previously showed that sclerostin neutralizing antibody (SclAb) treatment led to greater blood vessel density during bone healing in a mouse femoral osteotomy model (Kruck et al., 2018). No one has examined the effect of short-term sclerostin inhibition on vascular or lacunar microporosity during bone healing, although two studies have examined these properties in the absence of drug treatment (Casanova et al., 2021) (Schemenz et al., 2020). With the likely increased long-term and short-term clinical use of SclAb, especially in elderly population at risk for fracture, studies examining the safety of these drugs are needed.

In the current study, our primary aim was to examine the effect of *Sost* deficiency on bone mass and microstructure, in particular osteocyte lacunar and bone vascular properties, as a function of mouse age (10, 26, 78-week-old) and tissue age (endosteal, periosteal and intracortical bone). Our secondary aim was to report on osteocyte lacunar and bone vascular properties after short-term sclerostin deficiency in woven and cortical bone during osteotomy healing.

2. Methods

2.1. Animals

The sperm of four male *Sost*−/− mice (provided by Novartis) was pooled into two groups and intracytoplasmic sperm injection with the oocytes from female C57Bl/6J mice was performed. The first heterozygous generation was mated among themselves. In following generations, homozygous *Sost* KO and littermate control (LC) mice were identified using a Multiplex PCR with mice tail cuts, according to a protocol provided by Novartis. Three primers (*Sost*-specific endogen: 5′ TCC ACA ACC AGT CGG AGC TCA AGG 3′, *Sost*-specific endogen and target: 5′ ACT CCA CAC GGT CTG GAA AGT TTG G 3′ and Neo target: 5′ GGG TGG GAT TAG ATA AAT GCC TGC TCT 3′) were used to detect the homozygous LC (*Sost*-specific endogen – *Sost* –specific endogen and target) and *Sost* KO (Neo target – *Sost* -specific endogen and target) mice.

2.2. Experimental design

The study was approved by the local Animal Care and Use Committee (LaGeSo, Berlin, Germany; G0021/11). To examine the effect of long and short-term sclerostin deficiency on microporosity, we examined two different cohorts of mice. First, twenty-eight, female *Sost* KO and littermate control (LC), (C57BL/6J) mice (Jackson Laboratory, Sulzfeld, Germany) were aged to 10, 26, and 78 weeks of age (n = 4–5 mice/genotype/age) and then euthanized by cervical dislocation under isoflurane anesthesia and the tibia was dissected (Fig. 1 left). Although C57Bl6J mice have an average life span of 2 to 2.5 years, we chose 78 weeks of age as our oldest group in this study, since the Sost KO mice had an approximately 70% mortality rate at this age. Second, a separate cohort of ten, 26-week-old female C57BL/6J mice was randomly assigned to vehicle (veh) (n = 4) or sclerostin neutralizing antibody

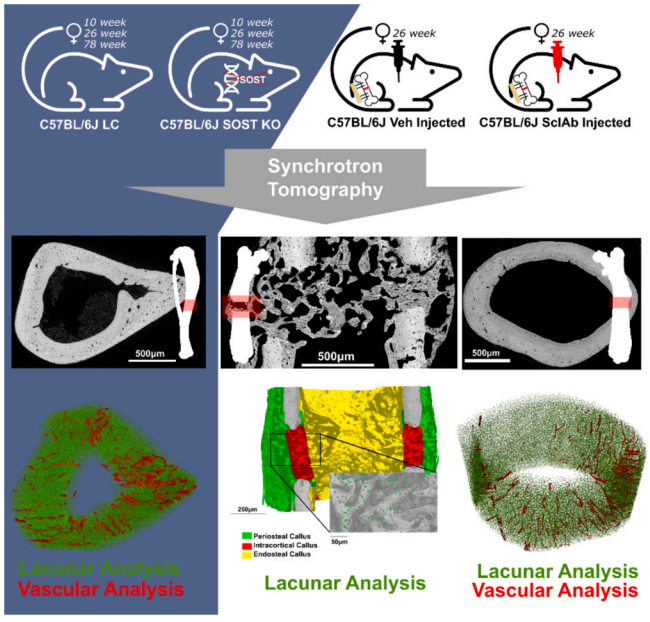

Fig. 1. Experimental design process. (dark blue) C57BL/6 J LC mice and *Sost* KO mice were aged to 10-, 26-, and 78 weeks and had their left tibiae scanned at the ESRF ID19 Beamline. Osteocyte lacunae and vascular canal porosity were analyzed. (white) 26-week old C57BL/6 J mice had an osteotomy performed on their left femur with the right serving as an internal control. Mice were either treated with Sclerostin neutralizing antibody or vehicle for 3 weeks. Left and right femora were scanned at PETRA III, P05 beamline. In the osteotomized femur the osteocyte lacunae were analyzed in the periosteal, intracortical and endocortical callus. In the intact femora the osteocyte lacunar and vascular canal porosity were analyzed.

(SclAb) ($n = 6$) groups. The mice underwent osteotomy surgery that has been described previously (Kruck et al., 2018), briefly, a 0.5-mm osteotomy was performed on the left femur and was stabilized with a rigid external fixator. Following surgery, mice were treated with subcutaneous injections 2×/week (1, 5, 8-, 12-, 15-, and 19-days post-osteotomy) of either ratized sclerostin monoclonal antibody (SclAb) (25 mg/kg, Scl-AbIII; Amgen Inc., USA, and UCB, Belgium) or saline solution (veh). Animals were euthanized by cervical dislocation under isoflurane anesthesia after 21 days of healing and the femora from both the operated and contralateral limb were dissected. The fixators were carefully removed from the operated femur, leaving the fracture callus available for high resolution 3D imaging (Fig. 1 right).

2.3. Phase contrast enhanced microtomography

Tibiae scanning: each tibial sample was fixed and sealed in ethanol-humidified plastic tubes and mounted onto sample stubs and scanned using phase-contrast micro-tomography (PCE-CT) at the beamline ID19 of the European Synchrotron Radiation Facility (ESRF, Grenoble, France) (Fig. 1 Left). An energy of 26.3 keV was used, taking 3600 radiographs over 360° of rotation in half-acquisition mode. An effective pixel size of 0.65 μm was achieved resulting in a field of view of 1.65 × 1.40 mm using a detector situated 14.5 mm behind the sample. All data were normalized and reconstructed using the pyHST interface (Mirone et al., 2013) accessed at the ANATOMIX beamline at Synchrotron SOLEIL (French national synchrotron facility, Saint-Aubin, France) using a Paganin phase retrieval algorithm with a unsharp filter of 3 and a strength of 0.8 and a Paganin length of 13 pixels.

Femora scanning: both healing and contralateral femora from each operated mouse were fixed in 10% neutrally buffered saline and transferred to Eppendorf tubes with ethanol vapor and stabilized with ethanol soaked styropor. Specimens were scanned by PCE-CT by using the Helmholtz-Zentrum Geesthacht operated, partial coherence, P05 imaging beamline of the Deutsches Elektronen-Synchrotron (DESY Hamburg, Germany) (Fig. 1 right). An energy of 22 keV was used, taking 1200 radiographs over 180°. An effective pixel size of 1.14 μm was achieved resulting in a field of view of 3.5 × 3.5 mm using a detector situated 25 mm behind the sample for phase contrast enhancement. All data were normalized and reconstructed using ring reduction algorithms (NRecon; Bruker CT, Kontich, Belgium).

2.4. Image analysis of lacunar and vascular porosity in the intact tibiae and contralateral femora

All images were loaded into Xamflow (1.9.7.0, Lucid Concepts, Zurich. Switzerland) and rotated along the main axis of the bone. Gaussian filters were applied to minimize noise in for segmentation of bone from background (Sigma 4, support 2), as well as for segmenting lacunae from the background. (Sigma 0.6, support 2). Similar regions of interest were extracted from the contralateral intact femurs as operated femurs (1 mm at midshaft of the bone). For tibiae, regions of interest of 0.8 mm were extracted, centered around the mid-diaphysis of the bone. A mask of the bone was created by thresholding the mineralized tissue and using morphological opening and closing to smooth the result and fill the lacunar and vascular pores. For both femora and tibiae, lacunae were segmented from the bone by using an isodata thresholding method as the phase retrieval imaging resulted in varying greyscale values across samples. The femurs and tibiae also had the bone segmented into primary quadrants for regional analyses, as well as separation of newly formed bone at endosteal and periosteal surfaces compared to mature bone at the intracortical region (Checa et al., 2015). Lacunae in each region were detected by filtering out pores between 50 and 2000 μm^3 (Goff et al., 2021; Mader et al., 2013). Pores larger than this, but still encapsulated within tissue, were considered vascular channels. The following osteocyte lacunar parameters were measured: lacunar number density (Lc.N/BV), individual lacunar volume (Lc.V), individual lacunar surface area (Lc.Sa), lacunar sphericity (Lc.Sr), lacunar angle (Lc.θ)-defined as the angle between the primary shape vector and the principal axis of the bone, lacunar equancy (Lc.Eq)– defined as the ratio of the largest shape vector to the smallest ranging from 0 (line) to 1 (perfect sphere), lacunar oblateness (Lc.Ob) – defined as a ratio of the 3 shape vectors resulting in values from −1 (rod shaped) to +1 (plate shaped), lacunar stretch (LcSt) - defined as the difference between the largest and smallest shape vectors, compared to the largest one, ranging from 0 (perfect sphere) to 1 (infinitely stretched), lacunar porosity (Lc. Po), as well as total lacunar volume (Lc.TV) (Goff et al., 2021; Mader et al., 2013). Vascular canals were classified as vascular canal thickness (V.·Th), vascular canal number (V·N), vascular canal separation (V.Sp) as well as vascular canal volume (V.·V), surface area (V.Sa) and vascular porosity (V.Po). All parameters are summarized in Table 1.

2.5. Image analysis of lacunar and vascular porosity in the operated femora after bone healing

All images were imported into Xamflow (1.9.7.0, Lucid Concepts, Zurich. Switzerland) and rotated along the main axis of the bone. Gaussian filters were applied as above. Regions of interest of 1 mm were

Table 1
List of parameters and abbreviations.

Parameter Name	Symbol	Description
Lacunar number density	Lc.N/BV	number of lacunae per unit volume
Individual lacunar volume	Lc.V	volume of an individual lacuna
Individual lacunar surface area	Lc.Sa	surface area of an individual lacuna
Lacunar sphericity	Lc.Sr	surface area to volume ratio
Lacunar angle	Lc.θ	angle between the primary shape vector and the principal axis of the bone
Lacunar angle standard deviation	Lc.θ.std	standard deviation of the mean lacunar angle to measure how aligned the principal axes of lacunae are
Lacunar equancy	Lc.Eq	the ratio of the largest shape vector to the smallest ranging from 0 (line) to 1 (perfect sphere)
Lacunar oblateness	Lc.Ob	a ratio of the 3 shape vectors resulting in values from −1 (rod shaped) to 1 (plate shaped)
Lacunar stretch	Lc.St	the difference between the largest and smallest shape vectors compared to the largest one ranging from 0 (perfect sphere) to 1 (infinitely stretched)
Lacunar total volume	Lc.TV	total volume of all lacunae in VOI
Lacunar porosity	Lc.Po	Lc.TV/BV
Vascular canal thickness	V.Th	average thickness (diameter) of a vascular canal
Vascular canal number	V.N	measured as 1/mm
Vascular canal separation	V.Sp	average distance between vascular canals
Vascular canal volume	V·V	total volume of all vessels in VOI
Vascular canal surface area	V.Sa	total surface area of all vessels in VOI
Vascular porosity	V·Po	V.V/BV
Cortical area	Ct.Ar	cross sectional area of bone
Marrow area	Ma.Ar	cross sectional area of marrow space
Total area	Tt.Ar	cross sectional area of the entire bone envelope
Cortical area fraction	Ct.Ar/Tt.Ar	ratio of cortical area to total area
Cortical thickness	Ct.Th	thickness of cortex
Imax	Imax	maximum second moment of inertia
Imin	Imin	minimum second moment of inertia
Periosteal Perimeter	Ps.Pm	circumference of periosteal surface
Endocortical Perimeter	Es·Pm	circumference of endocortical surface
Porosity	Po	porosity of bone

extracted, centered around the osteotomy. The intact parts of the femur were segmented due to the higher density, and interpolation was done to generate a total volume mask. This was also used to generate periosteal and endosteal regions of interest surrounding the bone.

Within the intact bone, a mask of the bone was created by thresholding the mineralized tissue and using morphological closing to fill the lacunar and vascular pores. Within the fracture callus, a mask of the callus was created by segmenting all mineralized tissue and subtracting the mask of the intact bone. Local thresholding was used to segment lacunae within the callus due to largely varying tissue densities within the tissue. Sub-analysis was done to analyze lacunae in the periosteal callus, endosteal callus and intracortical callus. Lacunar parameters were analyzed similar to intact tibia, as described above. The 50% mid-diaphysis of the contralateral femora were analyzed in the same manner as the tibiae described above.

2.6. Image analysis of microstructural parameters in the intact tibiae and femora

Masks of tibiae and femora from lacunar analysis were used to analyze microstructural parameters of the cortical bone. Cortical Area (Ct.Ar), total area (Tt.Ar) cortical area fraction (Ct.Ar/Tt.Ar), cortical thickness (Ct.Th), maximum area moment of inertia (Imax), minimum area moment of inertia (Imin), periosteal perimeter (Ps.Pm), endosteal perimeter (Es.Pm) and cortical porosity (Ct.Po) were measured.

2.7. Image analysis of microstructural parameters in operated femora after bone healing

Operated femurs were separated into quiescent bone volume (quiescent BV), mineralized callus volume (callus BV), and total callus volume (TV). The total volume was used to normalize bone volumes to calculate callus volume fracture (callus BV/TV), quiescent volume fraction (quiescent BV/TV), bone volume fraction (BV/TV).

2.8. Statistical analysis

All statistical analyses were performed in SAS (version 9.4, SAS Institute Inc.). To examine the effect of genotype and age in the tibiae, we used a 2-way ANOVA to compare genotype (*Sost* KO, LC) and age (10, 26, 78 weeks), as well as their interaction, with Tukey Kramer post hoc tests to explore genotype differences within ages as well as comparisons within each genotype between ages. A separate repeated measures ANOVA was performed to compare the effects of genotype (*Sost* KO, LC) age (10, 26, 78-week-old), and region (endocortical, intracortical and periosteal) as well as their interactions.

For the healing study we examined the intact femora by performing a Student *t*-tests to compare the effects of treatment (SclAb, veh). A repeated measures ANOVA was used to look at the effect of treatment (SclAb, veh), regions (newly formed endosteal and periosteal bone, quiescent intracortical bone) and their interaction. For the osteotomized femur, a 2- way ANOVA was also used to compare treatment (SclAb, vehicle), and tissue type (intact, callus) and their interaction.

For all analyses, a Tukey-Kramer post hoc tests were preformed for comparisons among groups. A p-value of <0.05 was considered significant and all data is presented as mean $\pm$ standard deviation in tables and graphs.

3. Results

3.1. Sost deficiency led to progressively enhanced cortical bone mass and microstructure with chronological aging, while LC mice had similar cortical outcomes across ages

Across the different ages (10, 26, and 78 weeks old), LC and *Sost* KO mice exhibited markedly different patterns of cortical bone mass and microstructure. *Sost* KO mice showed progressive and robust increases in nearly all bone microstructural outcomes with age. (Fig. 2) (Table 2) From 10 to 26 weeks, *Sost* KO mice demonstrated substantial growth, with greater Ct.Ar (45%) (Fig. 2 B), Tt.Ar (21%) (Fig. 1 B), Ct.Th (46%) (Fig. 1 B), and Ct.Ar/Tt.Ar (20%). Imax (52%), Imin (70%), and periosteal perimeter (10%) were also greater in 26-week-old compared to 10-week-old *Sost* KO mice. In *Sost* KO mice between 26 and 78 weeks, differences in bone mass and microstructure became even more pronounced. The Ct.Ar (55.3%), Tt.Ar (24%), Ct.Ar/Tt.Ar (24%), Ct.Th (66%), Imax (53%), and Imin (53%) were all greater at 78 compared to 26 weeks of age and Ma.Ar (−54%) was lower. Interestingly, periosteal perimeter was not significantly different between these two ages. From 10 to 78 weeks, *Sost* KO mice showed continuous cortical bone accrual, with Ct.Ar (125%), Ct.Th (142%), Tt.Ar (51%), Ct.Ar/Tt.Ar (48%), Imax (133%), and Imin (180%) all being greater at 78 compared to 10 weeks of age and Ma.Ar being lower (−60%). Periosteal perimeter was greater (18%) at 78 compared to 10 weeks of age, while endocortical perimeter was 52% lower at 78 compared to 26 weeks, and 46% lower at 78 weeks compared to 10 weeks *Sost* KO mice.

In contrast, in LC mice most structural parameters were greater in 26 compared to 10- or 78-week-old mice. Ct.Ar/Tt.Ar fraction was significantly greater (15%) in 26-week-old compared to 10-week-old mice. In contrast, Ct.Ar/Tt.Ar was lower (−19%) in 78 compared to 26-week-old mice with a higher Ma.Ar (21%). There were no differences between 10- and 78-week-old LC mice in any parameter. In summary, these results showed that Sost deletion led to sustained bone formation from 10 weeks up to 78 weeks of age, whereas wild-type littermate control mice experienced bone maturation followed by age-related decline.

3.2. Sost deficiency led to greater cortical bone mass and microstructure compared to LC mice at all ages

Across all ages examined, *Sost* KO mice consistently exhibit greater tibial cortical bone mass and geometry metrics compared to LC controls, with particularly larger differences between genotypes seen at older ages (Fig. 2 A) (Table 2). At 10 weeks, Ct.Ar (52%) (Fig. 2B), Tt.Ar (26%) (Fig. 2B), Ct.Th (43%), Ct.Ar/Tt.Ar (20%), and Imin (87%) were greater in *Sost* KO compared to LC mice. By 26 weeks, these differences intensified; Ct.Ar (82%), Tt.Ar (45%), Ct.Ar/Tt.Ar (25%), Ct.Th (73%) (Fig. 2B), Imax (103%), and Imin (144%) were greater in *Sost* KO compared to WT mice. At 78 weeks, the divergence was most pronounced; Ct.Ar (254%), Tt.Ar (86%), Ct.Ar/Tt.Ar (90%), Ct.Th (246%), Imax (358%), and Imin (334%) was greater in *Sost* KO compared to LC mice and Ma.Ar (−63%) was significantly lower. Periosteal perimeter was greater in *Sost* KO compared to LC mice at 26 weeks (12%) and at 78 weeks (28%), and endocortical perimeter was 45% lower at 78 weeks. Overall, these findings suggest that *Sost* deletion led to progressively amplified gains in bone mass, thickness, and structural strength with age compared to LC mice.

3.3. Sost deficiency led to altered osteocyte lacunae during chronological aging

Sost KO mice showed pronounced and distinctive differences in lacunar parameters at different ages. Although no significant differences in lacunar properties were measured between 10- and 26-week-old *Sost* KO mice, differences were observed between 26- and 78-week as well as 10-and 78-week-old *Sost* KO mice (Fig. 3A) (Table 3). Lacunar oblateness (20%) (Fig. 3B), lacunar angle (6%), lacunar angle standard deviation (13%) and lacunar total volume (30%) were all greater in 78-week-old *Sost* KO mice compared to 26-week-old *Sost* KO mice. The individual lacunar volume (−20%) (Fig. 3B) was lower with a corresponding lower lacunar surface area (−14%), as well as a lower porosity (−21.8%) (Fig. 3B), and lacunar angle (−7%) in 78-week-old compared to 10-week-old *Sost* KO mice. Despite lower lacunar size, the lacunar total volume (63%), oblateness (26%) (Fig. 3B) and the standard

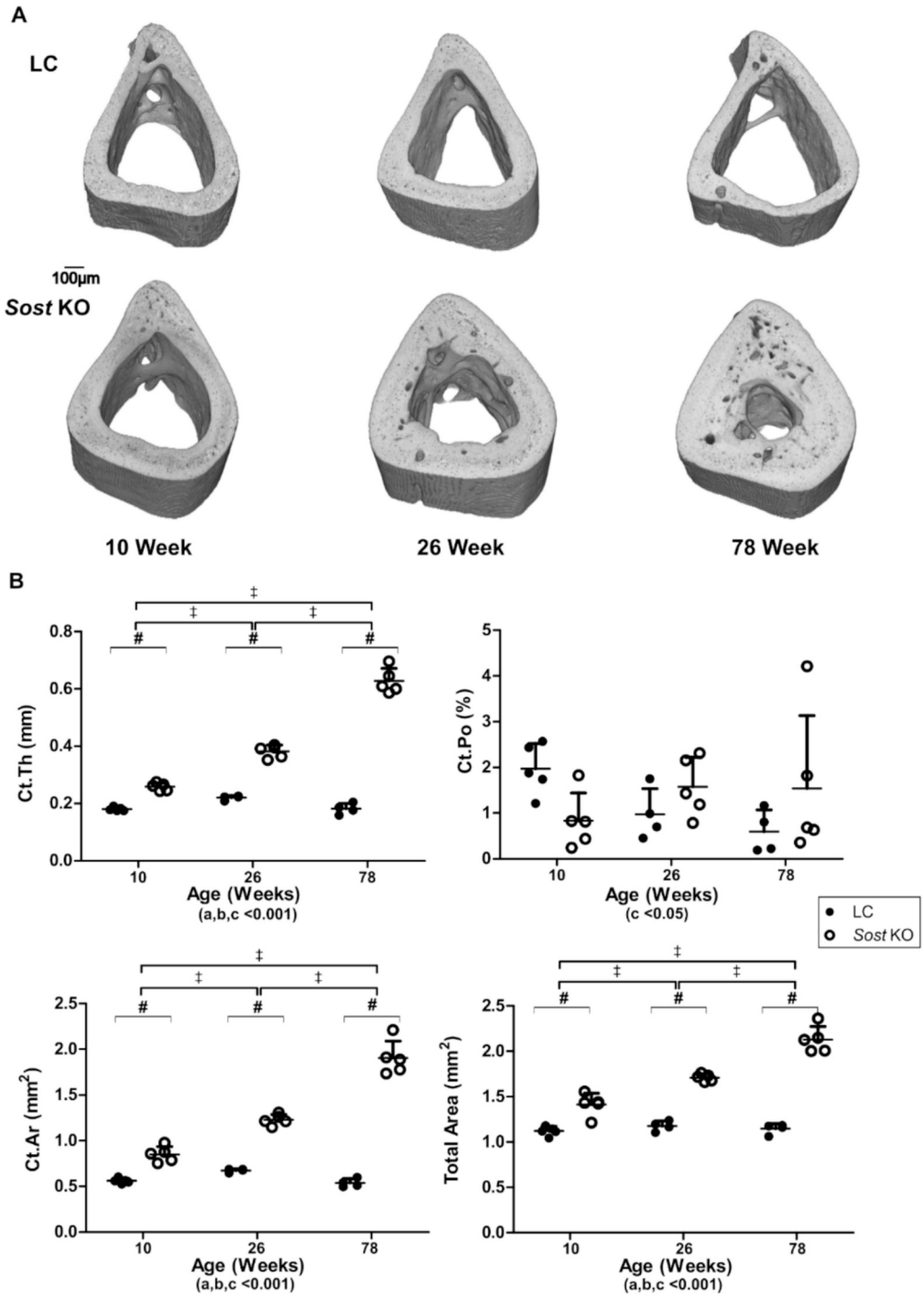

Fig. 2. Bone microstructural parameters. (A) 3D rendering example of the tibial mid-diaphysis of littermate controls (top) and *Sost* KO mice at 10 (left), 26 (middle) and 78 (right) weeks of age. (B) (top) Cortical thickness (left) and cortical porosity (right) and (bottom) cortical area (left) and cortical area fraction (right) in littermate controls (LC)(black circles) and *Sost* KO mice (white circles) at 10, 26 and 78 weeks of age. All data presented as means ± SD. ANOVA results a) genotype b) age c) interaction. # indicates $p < 0.05$ significance between genotypes via Tukey Kramer post hoc test. † Indicates $p < 0.05$ significance between ages in LC mice via Tukey Kramer post hoc test. ‡ Indicates $p < 0.05$ significance between ages in *Sost* KO mice via Tukey Kramer post hoc test.

deviation of the lacunar angle (17%) were greater in 78-week-old compared to 10-week-old *Sost* KO mice.

In contrast, in LC mice, 26-week-old mice had significantly lower lacunar number density (−14.7%) and lacunar porosity (−22.7%) compared to 10-week-old mice, while lacunar shape parameters were not different. Lacunar properties were not different between the 26- and 78-week-old LC mice. 78-week-old mice compared to 10-week-old mice had a lower lacunar density (5%) and a higher (7%) lacunar angle standard deviation.

In summary, total lacunar volume in *Sost* KO mice was 62.5% greater in 78-week-old compared to 10-week-old, but not different at these ages in LC mice. In general, aging in LC mice was marked by early structural compaction and porosity loss, while *Sost* KO mice exhibited preserved lacunar density, with gradual enlargement and reshaping of the lacunae with aging, suggesting divergent aging trajectories in lacunar properties between the genotypes.

Table 2
Tibial cortical bone microstructural parameters at 10, 26, and 78 weeks of age.

			10-Week-Old						26-Week-Old						78-Week-Old					
Parameters			LC			*Sost KO*			LC			*Sost KO*			LC			*Sost KO*		
Tibial cortical bone			n	=	5	n	=	5	n	=	4	n	=	5	n	=	4	n	=	5
Ct.Ar (mm^2)	a, b, c	*	0.56	±	0.03	0.85	±	0.09	0.67	±	0.02	1.23	±	0.06	0.54	±	0.05	1.91	±	0.19
Ma.Ar(mm^2)	a, b, c		0.56	±	0.03	0.56		0.07	0.50	±	0.04	0.48	±	0.05	0.61	±	0.06	0.22	±	0.05
Tt.Ar (mm^2)	a, b, c	*	1.12	±	0.05	1.41	±	0.12	1.18	±	0.06	1.71	±	0.04	1.15	±	0.06	2.13	±	0.15
Ct.Ar/Tt.Ar (mm^2/mm^2)	a, b, c	*	0.50	±	0.01	0.60	±	0.03	0.57	±	0.02	0.72	±	0.03	0.47	±	0.04	0.89	±	0.03
Ct.Th (mm)	a, b, c	*	0.18	±	0.01	0.26	±	0.01	0.22	±	0.01	0.38	±	0.02	0.18	±	0.02	0.63	±	0.04
Imax (mm^4)	a, b, c		0.14	±	0.01	0.21	±	0.06	0.16	±	0.01	0.32	±	0.04	0.11	±	0.01	0.49	±	0.08
Imin (mm^4)	a, b, c	*	0.05	±	0.00	0.10	±	0.01	0.07	±	0.01	0.17	±	0.01	0.06	±	0.01	0.28	±	0.04
Periosteal Perimeter (mm)	a, b, c		4.85		0.11	5.01		0.38	4.94	±	0.15	5.54	±	0.22	4.62	±	0.22	5.95	±	0.21
Endocortical Perimeter (mm)			3.65		0.16	3.36		0.30	3.22	±	0.24	3.80	±	0.48	3.34	±	0.33	3.46	±	1.44
Porosity (%)	c		1.97		0.55	0.83		0.61	0.97	±	0.56	1.57	±	0.65	0.59	±	0.47	1.54	±	1.59

ANOVA results a) genotype b) age c) interaction.
* Indicates $p < 0.05$ significance between genotypes via Tukey Kramer post hoc test.

3.4. Younger Sost deficient mice had altered osteocyte lacunae compared to LC mice

At 10 weeks of age, *Sost* KO mice had a greater individual lacunar volume (16%) (Fig. 3B) (Table 3), compared to LC. Lacunar stretch was lower (1.4%), and oblateness was less negative (18%) (Fig. 3B) (more spherical) in *Sost* KO compared to LC mice. In addition, equancy (7%) and lacunar angle standard deviation (7%) were greater in 10-week-old *Sost* KO compared to LC mice. Notably, lacunar porosity was similar, but total lacunar volume was greater (78%) in 10-week-old *Sost* KO compared to LC mice.

At 26 weeks, *Sost* KO mice had a greater (10%) lacunar number density, oblateness was less negative (20%), while sphericity was lower (3%) than in LC mice. Equancy (7%), lacunar angle standard deviation (8%), lacunar porosity (26%) and total lacunar volume (122%) were all greater in 26-week-old *Sost* KO compared to LC mice.

In 78-week-old mice, oblateness was less negative (31%) in *Sost* KO mice, with other shape parameters remaining similar to LC mice. Lacunar angle was lower (7%) with its standard deviation being higher (17%) in 78-week-old *Sost* compared to LC mice.

In summary, young and skeletally mature *Sost* KO mice displayed greater lacunar volume and shape differences compared to LC mice, with more similar lacunar properties between genotypes in elderly mice.

3.5. Sost deficiency led to greater vascular canal porosity with age

Sost KO mice exhibited substantial age-related increases in bone vascular pore properties (Fig. 4 A) (Table 4). No differences were measured between 10 and 26 weeks *Sost* KO mice. However, the vascular canal volume (100%) and surface area (74%) were greater in 78-week-old compared to 26-week-old *Sost* KO mice. The vascular volume (282%), surface area (161%), and vascular porosity (76%) were all greater in 78-week-old compared to 10-week-old *Sost* KO mice (Table 4).

In contrast, within the LC mice, most vascular parameters were lower with age, suggesting a decline in the vascular network of tibial cortical bone. Only the total microporosity – porosity from vasculature and lacunae combined - becomes significantly decreased (−26%) from 10 to 26 weeks. From 26 to 78 weeks there were no significant changes except for total microporosity (−23%) being lower.

In summary, the bone vascular pore properties indicate age-related vascular expansion within the Sost KO mice, suggesting a strong role for sclerostin in limiting both bone and vascular volume during aging.

3.6. Skeletally mature and elderly Sost KO mice had greater bone vascular pore properties than LC mice

At 26 and 78 weeks of age, *Sost* KO mice exhibited greater bone vascular pore properties in the tibial cortical bone compared to LC controls, while no differences were observed in 10-week-old mice (Fig. 4A) (Table 4). At 26 weeks of age, *Sost* KO mice showed markedly greater vascular thickness (88%) (Fig. 4B), vascular volume (298%), surface area (180%) with vascular porosity (115%) more than double that of LC mice. At 78 weeks of age, all vascular parameters were significantly greater in *Sost* KO compared to LC mice: vascular volume (1200%), surface area (700%), and vascular porosity (332%). In addition, vascular canal thickness (100%), and vascular number (37%) were greater in elderly *Sost* KO compared to LC mice, leading to a corresponding lower vascular canal separation (26%).

In summary, these bone vascular pore properties suggest that *Sost* deficiency led to progressively amplified vascularization with age, particularly in terms of vascular volume, porosity, and surface area.

3.7. Sost deficiency alters lacunar properties in periosteal newly formed bone more than endocortical newly formed bone

To examine site-specific effects of sclerostin deficiency, bone was

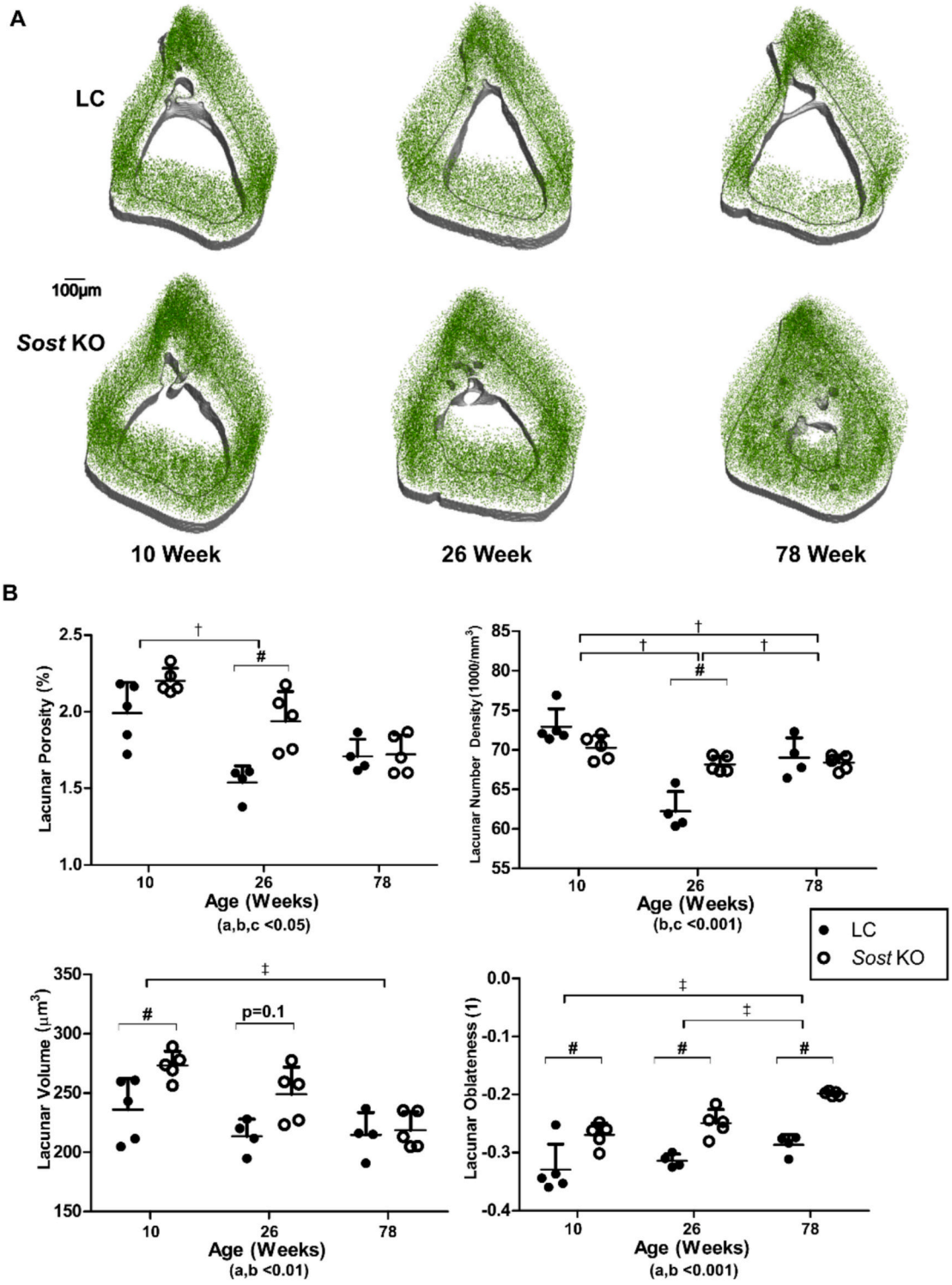

Fig. 3. Osteocyte lacunar parameters. (A) 3D renderings of the osteocyte lacunae and tibial mid diaphysis of littermate controls (top) and *Sost* KO mice at 10 (left) 26 (middle) and 78 (right) weeks of age. (B) (top) Lacunar porosity (left) and lacunar number density (right) and (bottom) lacunar volume (left) and lacunar oblateness (right) in littermate controls (black circles) and *Sost* KO mice (white circles) at 10 26 and 78 weeks of age. All data presented as means ± SD. ANOVA results a) genotype b) age c) interaction. # indicates $p < 0.05$ significance between genotypes via Tukey Kramer post hoc test. † Indicates $p < 0.05$ significance between ages in LC mice via Tukey Kramer post hoc test. ‡ Indicates $p < 0.05$ significance between ages in *Sost* KO mice via Tukey Kramer post hoc test.

segmented to analyze the 20 μm regions nearest to the endocortical and periosteal surfaces, since this region of each surface contains newly formed bone (Birkhold et al., 2016). No differences in lacunar properties were found between *Sost* KO and LC mice in the endocortical bone at 10 weeks of age or 78 weeks of age (Fig. 5). At 26 weeks, lacunar density (28%) and a lacunar porosity (47%) at the endocortical surface were greater in *Sost* KO compared to LC mice, pointing to significantly higher bone porosity and lacunar occupancy at skeletal maturity. These results suggest that skeletal maturity is a period of pronounced divergence in lacunar structure and porosity between genotypes in endocortical bone.

Table 3
Tibial cortical bone lacunar parameters at 10, 26, and 78 weeks of age.

Parameters			10-Week-Old						26-Week-Old						78-Week-Old					
			LC			*Sost KO*			LC			*Sost KO*			LC			*Sost KO*		
Tibial cortical bone			n	=	5	n	=	5	n	=	4	n	=	5	n	=	4	n	=	5
Lacunar Number Density (1000/mm^3)	b, c		72.92	±	2.26	70.27	±	1.52	* 62.23	±	2.49	68.17	±	1.01	69.02	±	2.52	68.38	±	0.96
Individual Lacunar Volume (μm^3)	a, b	*	235.97	±	26.48	273.33	±	11.98	213.61	±	14.24	248.95	±	23.05	214.69	±	18.91	218.69	±	15.38
Individual Lacunae Surface Area (μm^2)	a, b		262.03	±	22.00	285.46	±	8.52	243.75	±	11.76	266.83	±	17.32	243.55	±	15.68	246.14	±	12.35
Lacunar Stretch (1)	a	*	0.74	±	0.01	0.73	±	0.00	0.74	±	0.01	0.74	±	0.00	0.74	±	0.01	0.74	±	0.00
Lacunar Oblateness (1)	a, b	*	−0.33	±	0.04	−0.27	±	0.02	* −0.31	±	0.01	−0.25	±	0.02	* −0.29	±	0.02	−0.20	±	0.00
Lacunar Sphericity (1)	b		1.18	±	0.05	1.14	±	0.02	1.20	±	0.03	1.17	±	0.05	1.20	±	0.05	1.21	±	0.04
Lacunar Equancy (1)	a, c	*	0.14	±	0.01	0.15	±	0.004	0.14	±	0.01	0.15	±	0.003	0.15	±	0.01	0.15	±	0.004
Lacunar Angle (°)	a, b, c		157.57	±	0.80	155.11	±	1.19	* 156.57	±	1.67	152.67	±	1.93	* 154.41	±	1.85	144.24	±	1.90
Lacunar Angle Standard Deviation	a, b, c	*	23.25	±	0.48	24.94	±	0.70	* 23.98	±	0.79	25.91	±	0.64	* 24.93	±	0.89	29.34	±	0.67
Lacunar Porosity (%)	a, b, c		19.90	±	0.20	2.20	±	0.08	* 1.54	±	0.11	1.94	±	0.19	1.71	±	0.11	1.72	±	0.13
Lacunar Total Volume (mm^3)	a, b, c	*	0.009	±	0.001	0.016	±	0.002	* 0.009	±	0.001	0.020	±	0.003	* 0.008	±	0.001	0.026	±	0.005

ANOVA results a) genotype b) age c) interaction.
* Indicates $p < 0.05$ significance between genotypes via Tukey Kramer post hoc.

On the periosteal surface, 10-week-old *Sost* KO mice showed lower lacunar density (−22%), lacunar volume (−15%), lacunar area (−10%), and especially lacunar porosity (−33%) compared to LC mice, suggesting a less porous and smaller lacunar network early in life. Lacunar oblateness (−32%), was also dramatically lower indicating a more spherical lacuna shape in *Sost* KO mice than LC mice. At 26 weeks of age, lacunar density was no longer different between the two genotypes, but there appeared an even stronger size difference, with lacunar volume (−18%), lacunar area (−11%) and lacunar porosity (−19%) being lower in *Sost* KO compared to LC mice. Lacunar oblateness (−64%) was lower while sphericity was higher (6%), pointing to continued morphological divergence in lacunae shape and porosity. By 78 weeks, only lacunae oblateness was lower (−133%) in *Sost* KO compared to LC mice.

These findings suggest that *Sost* KO mice exhibit reduced lacunar complexity and porosity throughout life compared to LC mice, particularly during early and mid-adulthood, which may affect osteocyte function and bone remodeling. Sclerostin deficiency had a more remarkable effect on the periosteal surface compared to the endocortical surface.

3.8. *Sost deficiency altered bone vascular pore properties in newly formed bone on the periosteal and endocortical surfaces differently*

Within newly formed bone on the endocortical surface, no differences in bone vascular pore properties were found between *Sost* KO and LC in the 10- and 26-week-old mice (Fig. 6). However, in the 78-week-olds, the vessel separation was lower (49%), while the vessel number (114%) and the vessel porosity (366%) were greater in *Sost* KO compared to LC mice, resulting in a total microporosity (vascular canals and lacunae) also being higher (61%).

In the newly formed bone on the periosteal surface of the 10- and 26-week-old animals the vascular volume (−61%, −71%), surface area (−61%, −72%), porosity (−64%, −75%) and total microporosity (−39%, −33%) was markedly lower in the *Sost* KO mice compared to the LC mice. This difference continued with the vascular porosity being so low in the 78-week-old *Sost* KO mice that it could not be detected in most animals. Also, the thickness of vascular canals (−26%) was lower only in 26-week-olds *Sost* KO mice in the periosteal region.

In summary, these bone vascular pore properties suggest that the amount of vessel formation increases with age on the endocortical surface but decreases with age on the periosteal surface.

3.9. *Lacunar parameters in intracortical bone were similar between genotypes with age, while vascular parameters diverged between genotypes with age*

Although the intracortical region of mice has largely been considered quiescent, reports of old age leading to de novo intracortical remodeling (Piemontese et al., 2017) perilacunar remodeling around osteocytes, as well as recent evidence of intracortical remodeling around blood vessels in 26 old C57BL/6 mice (Ford et al., 2025) suggest the intracortical bone of mice is a more active region than previously thought. At 10 weeks of age, *Sost* KO mice showed greater lacunar volume (26%) (Fig. 5), lacunar area (15%), equancy (14%), lacunar porosity (16%), and lacunar angle standard deviation (8%), indicating more voluminous, porous, and less organized lacunae early in life compared to LC mice. Conversely, lower lacunar density (−6%), oblateness (−18%), sphericity (−7%), stretch (−2%), and angle (−2%) were observed in the intracortical region of 10-week-old *Sost* KO compared to LC mice, suggesting a shift toward fewer, and rounder lacunae.

By 26 weeks of age, lacunar volume (24%), lacunar area (13%), lacunar porosity (30%), lacunar total volume (219%), and lacunar angle standard deviation (11%), alongside greater equancy (13%), and sphericity (6%) remained greater in *Sost* KO compared to LC mice. Lower oblateness (−17%), and stretch (−2%) at this age indicated continued shape modification with *Sost* deficiency.

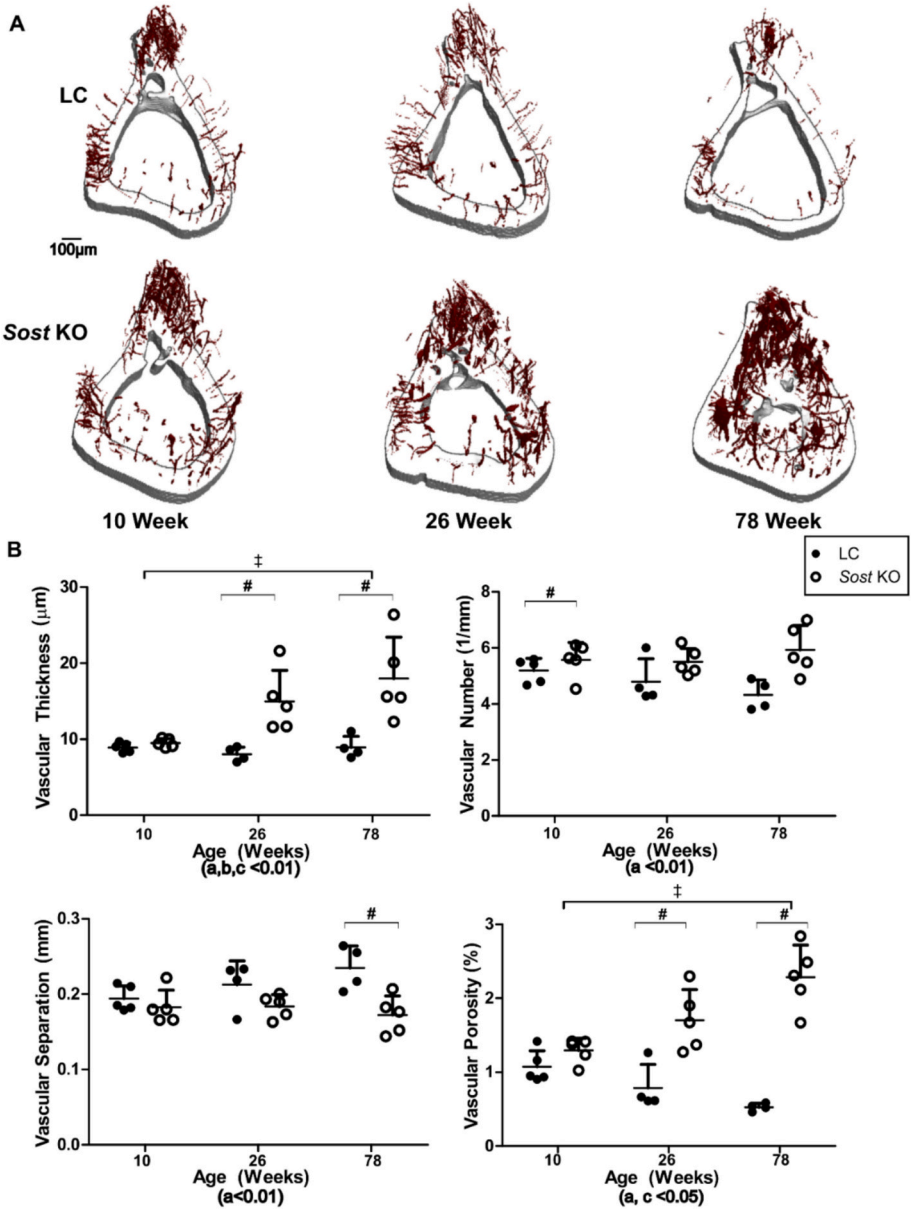

Fig. 4. Vascular canal properties. (A) 3D renderings of the tibial mid diaphysis of littermate controls (top) and *Sost* KO mice at 10 (left) 26 (middle) and 78 (right) weeks of age. (B) (top) vascular thickness (left) and vascular number density (right) and (bottom) vascular separation (left) and vascular porosity (right) in littermate controls (black circles) and *Sost* KO mice (white circles) at 10, 26, and 78 weeks of age. All data presented as means ± SD. ANOVA results a) genotype b) age c) interaction. # indicates $p < 0.05$ significance between genotypes via Tukey Kramer post hoc test. † Indicates $p < 0.05$ significance between ages in LC mice via Tukey Kramer post hoc test. ‡ Indicates $p < 0.05$ significance between ages in *Sost* KO mice via Tukey Kramer post hoc test.

At 78 weeks of age, some features reversed: lacunar porosity (−12%) and lacunar density (−13%) were lower in *Sost* KO mice compared to LC controls, while lacunar volume (2%), surface area (1%), and angle standard deviation (22%) remained greater. Oblateness (−32%), and equancy (−1%) were also lower, suggesting aging in *Sost* KO mice led to smaller, lesser lacunae that retained an irregular orientation. While lacunar porosity was lower, lacunar total volume was higher (458%) in *Sost* KO compared to LC mice, indicating that more lacunae were present within the greater bone tissue, but made up less of the porosity.

Overall, these findings suggest that *Sost* KO mice initially exhibit larger, more plentiful lacunae with altered geometry, but these differences attenuate or reverse with aging. Oblateness stands out as a parameter that consistently becomes more negative with aging.

At 10 weeks, no differences were found at the intracortical region between *Sost* KO mice and their LC controls in bone vascular pore properties. At 26 weeks, the differences intensified dramatically: vessel volume (458%), surface area (318%), vessel porosity (127%), vessel thickness (86%) and total microporosity (65%) were all greater suggesting a major expansion in vascular structure. At 78 weeks, the most extreme differences occurred: vessel volume (1300%), surface area (875%), vessel porosity (330%) and microporosity (70%) were all greater. Vessel thickness (103%) remained greater, and vessel number (43%) was greater, with a corresponding lower vessel separation (−29%) highlighting a profound age-related increase in vascularization in *Sost* KO compared to LC mice.

These results indicate that *Sost* KO mice develop a drastically more vascular and porous bone environment with age, particularly due to large increases in vessel volume and surface area, suggesting enhanced bone remodeling or altered angiogenesis.

Table 4
Tibial cortical bone vascular canal parameters at 10, 26, and 78 weeks of age.

			10-Week-Old						26-Week-Old						78-Week-Old					
Parameters			LC			*Sost KO*			LC			*Sost KO*			LC			*Sost KO*		
Tibial cortical bone			n	=	5	n	=	5	n	=	4	n	=	5	n	=	4	n	=	5
Vascular Thickness (mm)	a, b, c		0.009	±	0.001	0.010	±	0.001	0.008	±	0.001	0.015	±	0.004	0.009	±	0.001	0.018	±	0.005
Vascular Separation (mm)	a, c		0.194	±	0.02	0.18	±	0.02	0.21	±	0.03	0.18	±	0.02	0.23	±	0.03	0.17	±	0.03
Vascular Number (1/mm)	a		5.195	±	0.43	5.57	±	0.62	4.79	±	0.82	5.50	±	0.48	4.32	±	0.54	5.93	±	0.87
Vascular Volume (mm^3)	a, b, c		0.005	±	0.0009	0.0100	±	0.0020	0.0048	±	0.0018	0.0191	±	0.0051	0.0026	±	0.0002	0.0382	±	0.0118
Vascular Surface Area (mm^2)	a, b, c		2.021	±	0.35	3.68	±	0.65	1.97	±	0.90	5.52	±	1.18	0.99	±	0.14	9.62	±	3.27
Vascular Porosity (%)	a, b, c		1.074	±	0.22	1.30	±	0.17	0.79	±	0.32	1.70	±	0.42	0.53	±	0.05	2.29	±	0.44
Total Porosity (%)	a, b, c		2.854	±	0.26	3.36	±	0.19	2.10	±	0.14	3.35	±	0.36	2.18	±	0.11	3.70	±	0.37

ANOVA results a) genotype b) age c) interaction.
* Indicates $p < 0.05$ significance between genotypes via Tukey Kramer post hoc.

3.10. Three weeks of SclAb treatment altered bone vascular pore number, but not lacunar properties in quiescent bone from the intact femur of mice that had undergone an osteotomy in the contralateral femur

In contrast to the substantial changes seen in lacunar properties with a knockout of the *Sost* gene, the administration of three weeks of SclAb did not alter microstructural properties (Table 5), or lacunar properties (Table 6) compared to vehicle treatment in the contralateral limb. SclAb treatment did however have an impact on the mineralized vascular channels within the bone (Table 7). The vascular number (19%) was significantly lower in SclAb treated mice compared to vehicle-treated mice, with a corresponding trending greater vascular separation (23%) ($p = 0.06$). Vascular volume, surface area, and porosity all were trending lower with SclAb treatment (−16%, −26%, −25%), although large variance between samples likely prevented reaching statistical significance. Three weeks of treatment did not lead to altered bone microstructural parameters.

In summary, regardless of region analyzed (e.g. total callus mineralized volume, endocortical callus, periosteal callus), the data suggested that three weeks of SclAb administration had minimal impact on lacunar morphometry, although vascular number was lower in the femoral cortex, at 26 weeks of age. However, it should be noted that systemic inflammation or other systemic factors associated with bone healing occurring on the contralateral limb may have affected the lacunar or vascular properties within the intact limb.

3.11. Short-term SclAb treatment led to altered callus volume during bone healing, with no alteration to lacunar properties

The volume of callus and a mask of the entire bone envelope were used to calculate volumes. There was no difference in the mineralized callus bone volume (Supp Fig. 1). The callus BV/TV was significantly higher in the SclAb group compared to the vehicle injected controls. The lacunae within the callus were highly irregular and varied greatly in size and orientation depending on where they were located and the age of the tissue that they were embedded in. To try and compensate for these differences, lacunae within the callus tissue were analyzed globally, but were also separated into periosteal, intracortical, and endosteal callus (Fig. 7).

In summary, there were no differences in the lacunae within the fracture callus between treatments. There was a trend of lower lacunar density ($p = 0.09$) within the SclAb treated mice in the endosteal callus, which led also to a trend ($p = 0.09$) in lower lacunar porosity.

4. Discussion

This study evaluated the effects of *Sost* gene deletion and short-term sclerostin neutralization on cortical bone structure, osteocyte lacunar properties, and bone vascular pore properties across the murine lifespan. Our findings demonstrate that *Sost* deficiency led to progressive and robust increases in cortical bone geometry and microstructural complexity. The *Sost* knockout (*Sost* KO) phenotype is characterized by continued cortical bone accrual from 10 to 78 weeks, contrasting with the biphasic process of bone mass increases until skeletal maturity, and then decrease with aging observed in LC controls. These findings confirm previous work showing that sclerostin limits bone mass accrual in young and skeletally mature mice. Importantly, the present study, for the first time, reveals how *Sost* deficiency influences bone aging. In addition, our data shows that *Sost* deficiency leads to greater bone vascular porosity, but similar osteocyte lacunar properties with increasing age.

Sost KO mice exhibited sustained increases in cortical area (Ct.Ar), thickness (Ct.Th), and mechanical moments of inertia (Imax, Imin) throughout life, greatly decreasing the marrow area (Ma.Ar). These changes were most pronounced in older animals, where cortical area and cortical thickness were massively larger than in younger *Sost* KO

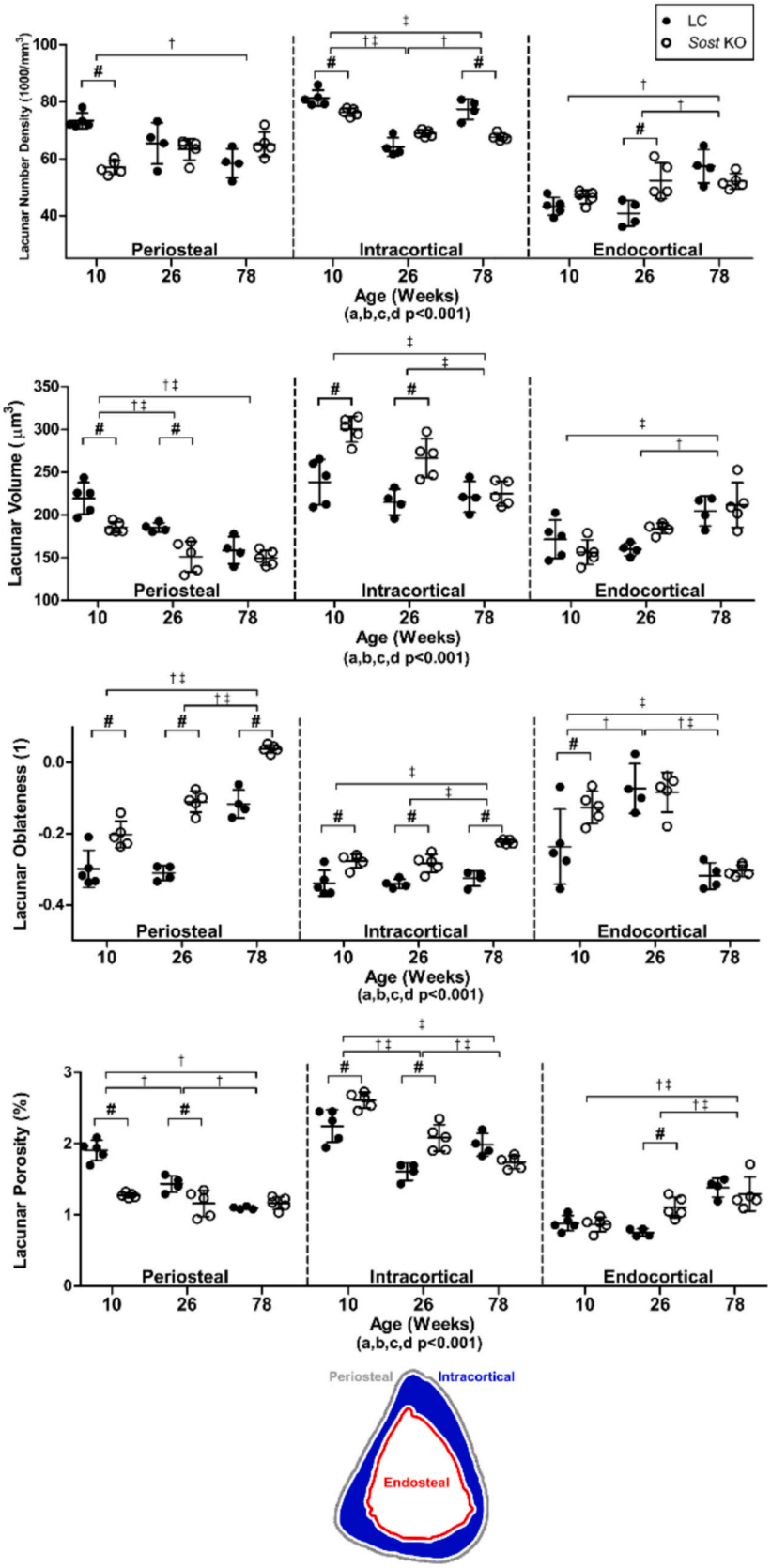

Fig. 5. Osteocyte lacunar parameters within regions of active (re)modeling (periosteal and endocortical) versus quiescent bone (intracortical). Lacunar number density, lacunar volume, lacunar oblateness, and lacunar porosity in the periosteal (right) intracortical (middle) and endocortical (right) regions in littermate controls (black circles) and *Sost* KO mice (white circles) at 10, 26 and 78 weeks of age. All data presented as means ± SD. ANOVA results a) region b) region *genotype c) region *age d) region*treatment*age. # indicates $p < 0.05$ significance between genotypes via Tukey Kramer post hoc test. † Indicates $p < 0.05$ significance between ages in LC mice via Tukey Kramer post hoc test. ‡ Indicates $p < 0.05$ significance between ages in *Sost* KO mice via Tukey Kramer post hoc test.

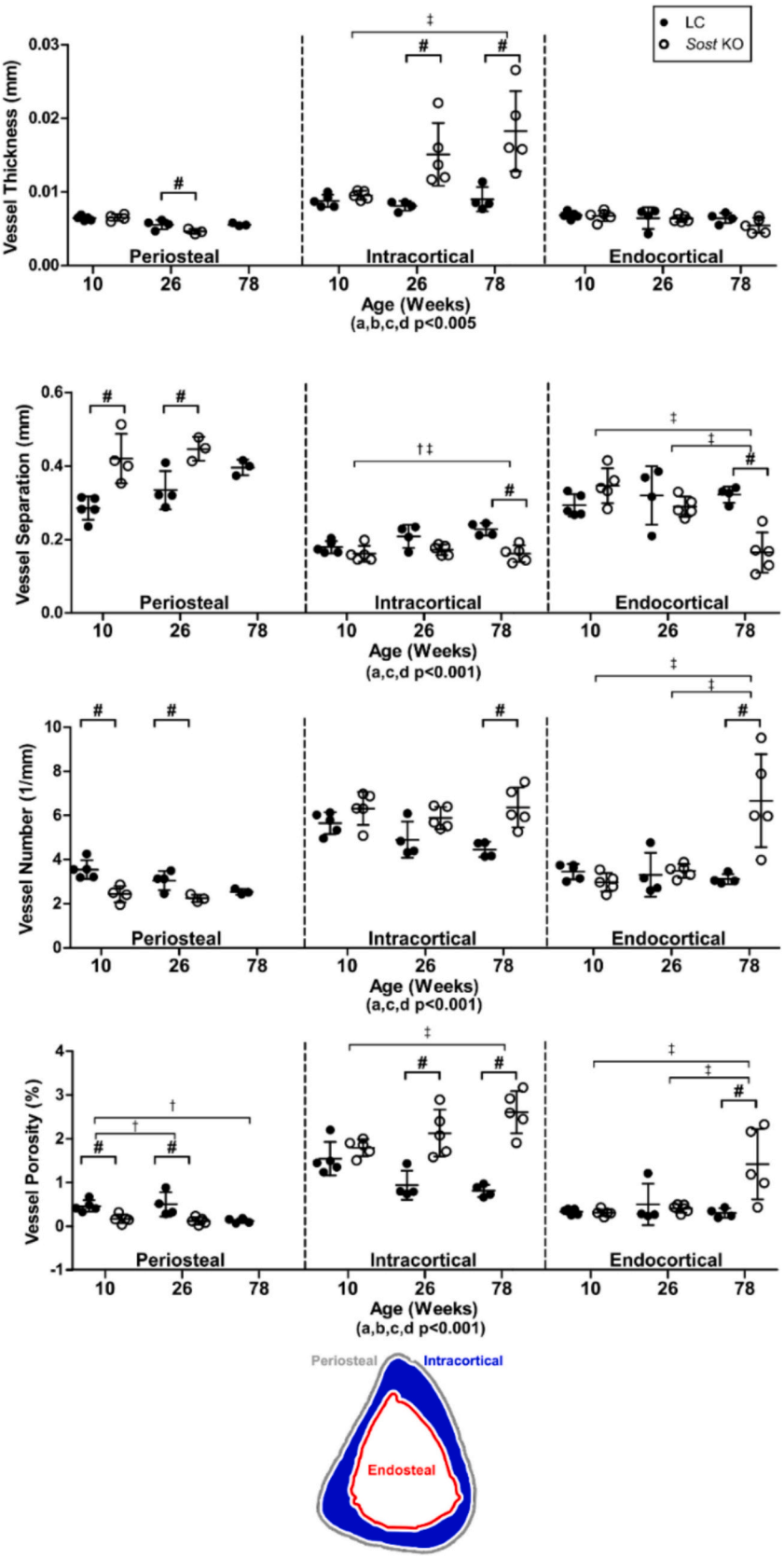

Fig. 6. Vascular channel parameters within regions of active (re)modeling (periosteal and endocortical) versus quiescent bone (intracortical). Vascular thickness, vascular separation, vascular number density, and vascular porosity in the periosteal (right) intracortical (middle) and endocortical (right) regions in littermate controls (black circles) and *Sost* KO mice (white circles) at 10, 26 and 78 weeks of age. All data presented as means ± SD. ANOVA results a) region b) region *genotype c) region *age d) region*treatment*age. # indicates $p < 0.05$ significance between genotypes via Tukey Kramer post hoc test. † Indicates $p < 0.05$ significance between ages in LC mice via Tukey Kramer post hoc test. ‡ Indicates $p < 0.05$ significance between ages in *Sost* KO mice via Tukey Kramer post hoc test.

Table 5
Contralateral femur cortical bone microstructural parameters after SclAb treatment or Vehicle.

	26-Week-Old					
Parameters	Veh			*SclAb*		
Femur Cortical Bone	n	=	7	n	=	6
Ct.Ar (mm^2)	1.00	±	0.09	0.97	±	0.12
Ma.Ar(mm^2)	0.98	±	0.10	0.88	±	0.06
Tt.Ar (mm^2)	1.89	±	0.06	1.95	±	0.10
Ct.Ar/Tt.Ar (mm^2/mm^2)	0.53	±	0.04	0.50	±	0.05
Ct.Th (mm)	0.25	±	0.02	0.24	±	0.03
Imax (mm^4)	0.31	±	0.03	0.32	±	0.04
Imin (mm^4)	0.16	±	0.01	0.16	±	0.02
Periosteal Perimeter (mm)	5.40	±	0.10	5.48	±	0.12
Endocortical Perimeter (mm)	3.86	±	0.12	4.01	±	0.22
Porosity (%)	0.21	±	0.06	0.16	±	0.03

Indicates $p < 0.05$ significance between genotypes via Tukey Kramer post hoc. No significance was measured.

Table 6
Contralateral femur cortical bone lacunar parameters after SclAb treatment or Vehicle.

	26-Week-Old					
Parameters	Veh			*SclAb*		
Femur Cortical Bone	n	=	7	n	=	6
Lacunar Number Density (1000/mm^3)	58.95	±	2.17	57.51	±	1.46
Individual Lacunar Volume (μm^3)	252.76	±	12.95	255.45	±	14.61
Individual Lacunae Surface Area (μm^2)	255.45	±	10.17	258.70	±	17.76
Lacunar Stretch (1)	0.69	±	0.03	0.70	±	0.03
Lacunar Oblateness (1)	−0.24	±	0.04	−0.22	±	0.06
Lacunar Sphericity (1)	1.05	±	0.04	1.06	±	0.03
Lacunar Equancy (1)	0.21	±	0.04	0.20	±	0.04
Lacunar Angle (°)	150.89	±	2.05	151.56	±	0.98
Lacunar Angle Standard Deviation	26.20	±	0.80	25.81	±	0.65
Lacunar Porosity (%)	1.62	±	0.10	1.61	±	0.10
Lacunar Total Volume (mm^3)	0.014	±	0.001	0.014	±	0.001

Indicates $p < 0.05$ significance between genotypes via Tukey Kramer post hoc. No significant differences were measured.

Table 7
Contralateral femur cortical bone vascular canal parameters after SclAb treatment or Vehicle.

		26-Week-Old					
Parameters		Veh			*SclAb*		
Femur Cortical Bone		n	=	7	n	=	6
Vascular Thickness (mm)		0.008	±	0.001	0.009	±	0.000
Vascular Separation (mm)		0.22	±	0.04	0.27	±	0.04
Vascular Number (1/mm)	*	4.69	±	0.77	3.78	±	0.56
Vascular Volume (mm^3)		0.0044	±	0.0012	0.0037	±	0.0008
Vascular Surface Area (mm^2)		1.73	±	0.63	1.28	±	0.36
Vascular Porosity (%)		0.47	±	0.11	0.40	±	0.11
Total Porosity (%)		2.04	±	0.19	2.05	±	0.20

* Indicates $p < 0.05$ significance between genotypes via Tukey Kramer post hoc.

mice. In contrast, LC mice displayed modest cortical area fraction gains from 10 to 26 weeks, followed by deterioration from 26 to 78 weeks—consistent with age-related bone loss (Birkhold et al., 2014; Willie et al., 2013). This follows the trends found by others as mice are constantly growing, even after they reach peak bone mass and skeletal maturity at 26 weeks of age (Ferguson et al., 2003). These changes are generally more pronounced in females (Glatt et al., 2007). This divergence suggests that sclerostin plays a central role in limiting bone accrual and mediating age-associated cortical thinning. The prolonged absence of sclerostin (*Sost* KO) causes an extreme amount of bone mass to be present at each age, increasing in severity with age, similar to previous studies (Albiol et al., 2020; Li et al., 2008). Our data shows that *Sost* KO mice continue to have increased bone formation even as mice age to 78 weeks, whereas LC mice see declines in bone formation.

In our study, chronological aging in both genotypes (*Sost* KO, LC) led to lacunar density, volume, and porosity decreases with age and oblateness to increase with age. However, as these values were already higher in the *Sost* KO mice at 10 weeks of age, the changes were more pronounced than in LC mice. While lacunar volume, density, and porosity were higher in *Sost* KO compared to LC mice at 10 and 26 weeks of age, these differences were no longer present by 78 weeks. Similar to what others have seen, the overall osteocyte lacunar number density decreases with age (Tiede-Lewis and Dallas, 2019) whether or not sclerostin levels are altered. Sclerostin may also be a controller of osteocytic osteolysis and perilacunar remodeling, with increasing levels resulting in higher levels of perilacunar resorption (Delgado-Calle et al., 2016). While some have seen no changes to lacunar volume due to aging, (Tiede-Lewis et al., 2017) others have shown decreases in lacunar volume with aging (Hemmatian et al., 2018).

Lactation and alteration of PTH levels have been shown to cause alterations to lacunar volume through perilacunar remodeling (Qing et al., 2012). Sclerostin binds to Wnt co-receptors LRP5 and 6 and prevents Wnt ligands from activating canonical Wnt/B-catenin signaling causing reduced osteoblast differentiation, activity, and bone formation and well as increasing osteoblast apoptosis (Compton and Lee, 2014). Importantly, there is evidence suggesting that perilacunar remodeling is influenced by developmental programs governed partly by Wnt signaling (Moharrer and Boerckel, 2021; Wang et al., 2021). In addition, sclerostin upregulates enzymes involved in bone matrix degradation (e.g. cathepsin K, carbonic anhydrase 2, and tartrate-resistant acid phosphatase), and exogenous sclerostin application to human trabecular bone cultures ex-vivo has been shown to increase lacunar size (Kogawa et al., 2013, 2018), further suggesting it influences osteocytic osteolysis.

Sost KO mice appear to have larger lacunae than their LC counterparts, indicating other pathways may be contributing to these volumetric changes. As the volumetric differences disappear in older animals, the hormonal declines in older animals that drive perilacunar remodeling may be the predominant signal, limiting the effect the *Sost* KO has on the lacunar volume at this age. Alternatively, it is possible that PCE-CT is not sensitive enough to detect micropetrosis and empty lacunae. As micropetrosis and osteocyte death increase with age, it is possible that there is another driving factor causing lacunar volume to decrease with age, with or without a decreased sclerostin level.

Interestingly, these differences were opposite and more pronounced at the periosteal surface, where *Sost* KO mice showed reduced lacunar density, volume, and porosity early in life, which reached similar levels to the LC by 78 weeks of age. The lacunar oblateness however, followed similar trends to the full volume, diverging more from LC with age and the oblateness continued to become less negative.

As periosteal apposition seems to be the main contributing factor to the higher bone mass in *Sost* KO mice, this may indicate that the rapid apposition on the periosteal surface leads to smaller lacunae. The lacunae then could undergo perilacunar remodeling in the intracortical bone, becoming larger. Sclerostin can inhibit mineralization and induce perilacunar remodeling which would explain these larger lacunae (Prideaux et al., 2016). This suggests that sclerostin plays a more prominent regulatory role in areas of active bone formation and apposition, particularly during midlife. The lacunar density was largely unaffected due to the KO in the periosteal and endocortical regions but was

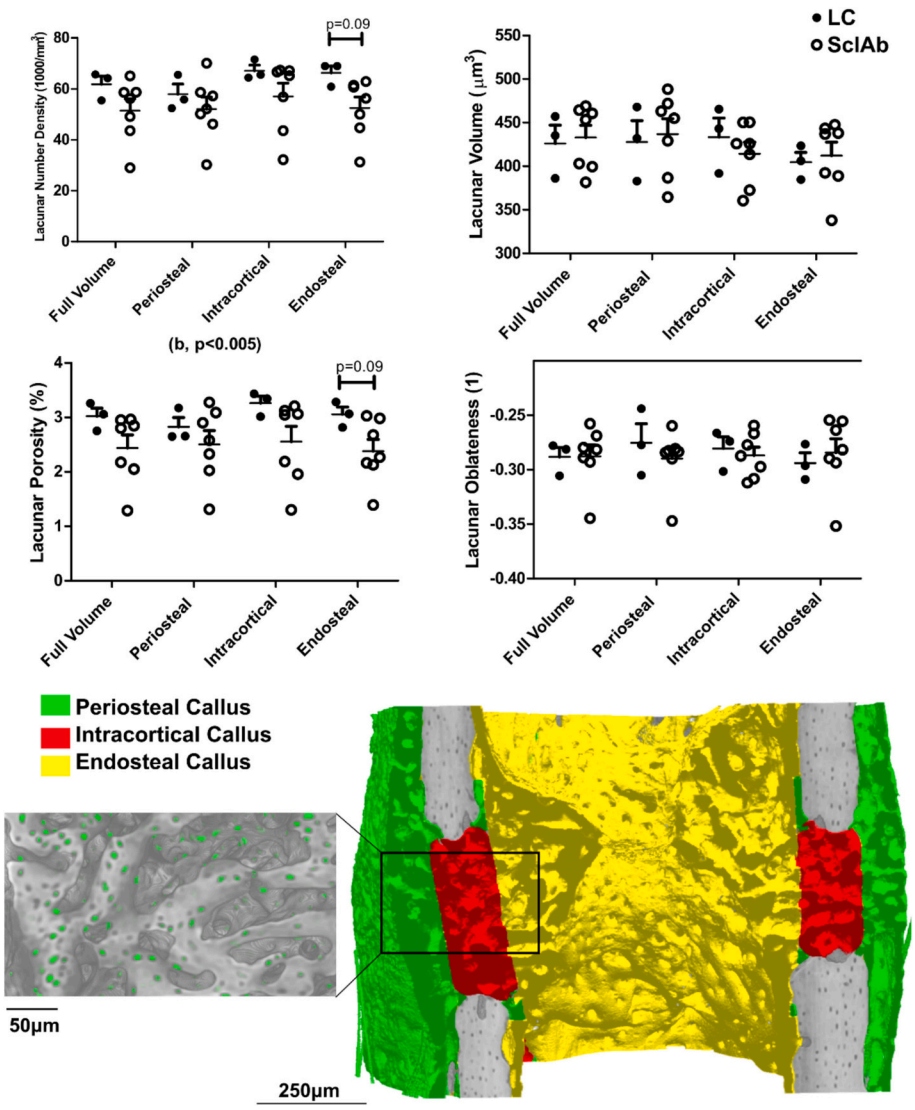

Fig. 7. Lacunar parameters measured in bone volumes of the healing callus separated into the periosteal callus, intracortical callus and endosteal callus as per the 3D rendering (bottom). Lacunar density, individual lacunar volume, lacunar porosity and lacunar oblateness in vehicle treated (black circles) and SclAb treated mice (white circles) All data presented as means ± SD. * indicates $p < 0.05$ significance between groups from a Students *t*-test.

altered in the intracortical region. This may indicate that bone formation is occurring normally, just more rapidly in *Sost* KO compared to LC mice. The lower lacunar density in the intracortical region at 10 and 78 weeks may also indicate that more osteocyte apoptosis occurs in *Sost* KO mice, or that more bone per osteoblast is laid down, resulting in less cells per mineralized matrix. The vascularity within the intracortical bone follows similar trends to the full volume with the thickness and porosity of vessels increasing with age. Within the periosteal region of the bone the vessel separation was greater in the *Sost* KO mice at 10 and 26 weeks with a corresponding lesser vessel number and porosity. The lower number of vessels in this region was even more pronounced at 78 weeks of age with none being detected within the *Sost* KO group. This is interesting as depleting the Wnt inhibiting sclerostin should allow for more angiogenesis (Olsen et al., 2017). This reinforces the idea that lacunar and vascular compartments respond differently to *Sost* deficiency.

In all cases the lacunae in the *Sost* KO mice had a higher oblateness, indicating the knockout impacted the shape of the lacunae making them more plate-like. Despite this, the trend of higher oblateness with age was seen in both genotypes, following what others have seen in male C57Bl/6 J mice between 6, 18, and 24 months with osteocytes becoming significantly less oblate with age (Heveran et al., 2018).

A striking phenotype in *Sost* KO mice was the progressive expansion of vascular canal networks with age, particularly between 26 and 78 weeks. Vascular volume, surface area, and porosity increased dramatically, in some cases over 10-fold, suggesting a potent role for sclerostin in limiting vascularization within cortical bone. This expansion was especially apparent in the intracortical and endocortical compartments of older mice, whereas vascular features in LC mice declined with age. Interestingly, periosteal vascularization was reduced or absent in *Sost* KO mice, pointing to regional differences in the effects of sclerostin. Sclerostin is an inhibitor of angiogenesis, and a knockout allows for more angiogenesis (Huang et al., 2024). As the Wnt signaling pathway is important for angiogenesis (Olsen et al., 2017), depleting sclerostin (a Wnt inhibitor) could allow for more angiogenesis, as more bone tissue forms. The coordinated increase in both bone and vascular volume in *Sost* KO animals suggests a potentially integrated remodeling response, possibly mediated by shared regulatory pathways for angiogenesis and osteogenesis. While PCE-CT does not allow confirmation of vasculature within these pores, it has been shown that pores over the size of lacunae often contain vessels (Núñez et al., 2017). However, without performing additional histology it is not possible to confirm that all the increased

porosity is from increased vasculature, and not trabecularization.

Short-term treatment with sclerostin-neutralizing antibody induced only modest changes compared to the dramatic lifelong effects of genetic deletion. While three weeks of SclAb treatment was not enough to impact lacunar parameters, it was enough to increase the number density of vascular channels overall with a modestly lower ($p = 0.06$) vascular separation and a modestly lower ($p = 0.09$) vascular channel thickness as well as an overall greater porosity not created from vessels or lacunae. This is in contrast to Qin et al. who found that SclAb could be used to combat bone loss from a long term spinal cord injury, by combatting the loss in osteocyte density and change of shape due to disuse (Qin et al., 2015). However, these findings were reported in rats who were treated for longer (7 weeks) in an unloading model. These differences may highlight the importance of duration of treatment, or also species-specific effects of treatment.

When the cortex was evaluated regionally, it appeared that the lower vascular thickness was coming predominantly from newly formed bone on the endosteal surface, with smaller vessels occurring in this region. The majority of osseous blood vessels within the cortex of murine bones are in the fibrolamellar intracortical band (Shipov et al., 2013) with fewer being found in the organized lamellar bone on the surfaces. This may contribute to the lesser vascular parameters in the new bone, especially that formed while SclAb inhibition was in effect.

During fracture healing, SclAb treatment significantly increased mineralized callus fraction (BV/TV), without affecting lacunar properties, indicating a rapid effect on mineralization, but not on cellular-level bone organization. The expression of *SOST* in humans is high in fracture sites (Sarahrudi et al., 2012). While the callus volume and the callus volume fraction were greater with the use of SclAb similar to others (Alaee et al., 2014; Virk et al., 2013), the volume and shape of individual lacunae within the callus did not change. Casanova et al. (Casanova et al., 2021) showed that lacunar volume decreases over time in woven bone within the callus and lacunar volume is larger in callus tissue than intact bone, with the lacunar density decreasing as the callus matures. We previously showed that lacunae in callus tissue have 34% higher lacunar density and 40% larger lacunar volume compared to those residing in the original cortical bone, indicating that the osteocyte-lacuno-canalicular network (OLCN) is different in healing versus quiescent bone.

There was also a modest ($p = 0.07$) decrease in lacunar porosity in the SclAb treated mice, which may come from this slightly lower lacunar density as lacunar volumes were not altered. When the callus was separated into various regions, analysis of the endosteal callus in the SclAb-treated mice was lower than vehicle-treated mice. This resulted in a lower lacunar porosity in this region as well. The lacunar porosity was also lower in the intracortical callus in the SclAb-treated mice. These findings suggest that SclAb may require longer or earlier treatment windows to elicit microstructural changes comparable to *Sost* deletion.

An important implication of the observed changes in microporosity is its potential contribution to bone fracture toughness. Microporosity plays a dual role in bone mechanics: while excessive porosity can compromise structural integrity (De Paolis et al., 2021; Ugarteburu et al., 2025) (Kaya et al., 2017), a well-organized microporous network can enhance toughness by promoting energy dissipation, crack deflection, and stress redistribution during loading (Carriero et al., 2014b). When bone is loaded, the strain surrounding osteocyte lacunae can be orders of magnitude higher than what the gross tissue experiences (Nicolella et al., 2005). Too large an increase in vascular porosity hinders crack deflection and cracks can propagate transversely through the canals rather than being deflected (Carriero et al., 2014a). Lacunae also naturally become more oblate with age and more disorganized with age, which may cause the tissue to become more brittle and less resistant to cracks (Muñoz et al., 2025b). Aging naturally causes an increase in vascular porosity, through increased vascular diameters, but not numbers (Andronowski et al., 2023). In contrast to this, lacunae are smaller and less round and lacunar and canalicular density are decreased (Andronowski et al., 2023; Heveran et al., 2018). An increased vascular porosity would contribute to fragility and a reduced, less connected OLCN would have less mechanosensitivity and ability to repair and reinforce bone due to this fragility (Andronowski et al., 2023).

LC mice exhibit early lacunar compaction and declining vascular porosity with age—hallmarks of more brittle bone prone to fracture. The *Sost* KO mice had even more pronounced lacunar oblateness changes and lacunar angle standard deviation increases with age, along with a greatly increased vascular porosity, which may support greater fracture resistance by providing microscale heterogeneity that hinders crack propagation. However, it is possible that this may have gone too far, and the bone may have become more brittle due to the large vascular and lacunar changes due to long-term sclerostin inhibition.

The current study is limited in that we did not measure fracture toughness in the mice, and the study was cross-sectional rather than longitudinal. However, our findings align with prior work linking reduced porosity and lacunar density to increased bone fragility in aged and osteoporotic bone (Bernhard et al., 2013). Thus, the enhanced and sustained porosity in sclerostin deficient mice may represent a mechanistic contributor to improved fracture toughness. However, further studies directly examining fracture toughness in sclerostin deficient mice bone and human bone biopsies are warranted to confirm this assertion to determine if this is a novel benefit of long-term sclerostin inhibition beyond bone mass accrual. It would also be important to study the underlying molecular mechanisms responsible for sclerostin inhibition altering cortical porosity. Another limitation is that we did not examine lacunar or vascular properties or explore gene or protein expression in young and old WT mice with SclAb treatment. Future studies are warranted to examine if short-term or long-term treatment with SclAb in WT mice leads to similar age-related effects shown with *Sost* deficiency. Lastly, due to the limited beam-time available at the synchrotron radiation facility, this study only focused on cortical bone in female mice to allow for a wider range of ages to be analyzed. Thus, future investigations should also examine trabecular bone and explore the effect of *Sost* deficiency in males.

5. Conclusion

Collectively, our data highlight the lifelong impact of *Sost* deficiency on bone mass, microstructure, and vascularity. *Sost* KO mice exhibit sustained cortical thickening and pronounced vascularization, particularly in aging bone. Short-term SclAb treatment, while beneficial for enhancing callus mineralization, fails to recapitulate the full microarchitectural changes seen in genetic deletion, suggesting that timing and duration are critical for therapeutic efficacy. Overall, this work underscores the multi-faceted role of sclerostin in regulating cortical bone integrity and aging, providing insights for both fundamental skeletal biology and the development of bone anabolic therapies.

CRediT authorship contribution statement

Taylor deVet: Writing – review & editing, Writing – original draft, Visualization, Validation, Software, Project administration, Methodology, Investigation, Formal analysis, Data curation. **Anthony Helou:** Writing – review & editing, Methodology, Formal analysis. **Sara Checa:** Writing – review & editing, Resources, Methodology. **Alexander Rack:** Writing – review & editing, Resources, Methodology. **Ina Kramer:** Writing – review & editing. **Fabian Wilde:** Writing – review & editing, Methodology. **Paul Zaslansky:** Writing – review & editing, Supervision, Resources, Funding acquisition, Formal analysis, Data curation, Conceptualization. **Bettina M. Willie:** Writing – review & editing, Writing – original draft, Validation, Supervision, Resources, Project administration, Methodology, Investigation, Funding acquisition, Formal analysis, Data curation, Conceptualization.

Declaration of competing interest

The authors declare the following financial interests/personal relationships which may be considered as potential competing interests: Bettina Willie reports equipment, drugs, or supplies was provided by Novartis Institutes for BioMedical Research Inc. Bettina Willie reports equipment, drugs, or supplies was provided by Amgen Inc. Bettina Willie reports a relationship with Angitia Inc. LTD. that includes: consulting or advisory and funding grants. If there are other authors, they declare that they have no known competing financial interests or personal relationships that could have appeared to influence the work reported in this paper.

Acknowledgments

We would like to thank the ESRF for funded beamtime on ID19 under proposal number IH-LS-2375. Also, we thank Dr. Julia Herzan for assistance in using the DESY Petra III P05 beamline with access under proposal I-20130007 and I-20140705. We would also like to thank Andy King at the SOLEIL Synchrotron for his help with data reconstruction. We also thank Amgen Inc. (Thousand Oaks, CA, USA) and UCB (Brussels, Belgium) for providing the sclerostin neutralizing antibody. We thank Dr. Michaela Kneissel, Novartis Biomedical Research, Switzerland for providing the initial four male *Sost* KO mice that underwent embryo transfer. Lastly, we thank the CIHR PJT 178048 and Shriner Hospitals for Children 206717 for funding.

Appendix A. Supplementary data

Supplementary data to this article can be found online at https://doi.org/10.1016/j.bonr.2026.101937.

Data availability

Data will be made available on request.

References

Alaee, F., Virk, M.S., Tang, H., Sugiyama, O., Adams, D.J., Stolina, M., Dwyer, D., Ominsky, M.S., Ke, H.Z., Lieberman, J.R., 2014. Evaluation of the effects of systemic treatment with a sclerostin neutralizing antibody on bone repair in a rat femoral defect model. J. Orthop. Res. 32 (2), 197–203. https://doi.org/10.1002/JOR.22498.

Albiol, L., Büttner, A., Pflanz, D., Mikolajewicz, N., Birkhold, A.I., Kramer, I., Kneissel, M., Duda, G.N., Checa, S., Willie, B.M., 2020. Effects of long-term Sclerostin deficiency on trabecular Bone mass and adaption to limb loading differ in male and female mice. Calcif. Tissue Int. 106 (4), 415–430. https://doi.org/10.1007/s00223-019-00648-4.

Andronowski, J.M., Cole, M.E., Davis, R.A., Tubo, G.R., Taylor, J.T., Cooper, D.M.L., 2023. A multimodal 3D imaging approach of pore networks in the human femur to assess age-associated vascular expansion and lacuno-canalicular reduction. Anat. Rec. (Hoboken, N.J.: 2007) 306 (3), 475–493. https://doi.org/10.1002/AR.25089.

Bernhard, A., Milovanovic, P., Zimmermann, E.A., Hahn, M., Djonic, D., Krause, M., Breer, S., Püschel, K., Djuric, M., Amling, M., Busse, B., 2013. Micro-morphological properties of osteons reveal changes in cortical bone stability during aging, osteoporosis, and bisphosphonate treatment in women. Osteoporos. Int. 24 (10), 2671–2680. https://doi.org/10.1007/S00198-013-2374-X/FIGURES/3.

Bhandari, M., Schemitsch, E.H., Karachalios, T., Sancheti, P., Poolman, R.W., Caminis, J., Daizadeh, N., Dent-Acosta, R.E., Egbuna, O., Chines, A., Miclau, T., 2020. Romosozumab in skeletally mature adults with a fresh unilateral tibial diaphyseal fracture a randomized phase-2 study. J. Bone Joint Surg. 102 (16), 1416–1426. https://doi.org/10.2106/JBJS.19.01008.

Birkhold, A.I., Razi, H., Duda, G.N., Weinkamer, R., Checa, S., Willie, B.M., 2014. The influence of age on adaptive bone formation and bone resorption. Biomaterials 35 (34), 9290–9301. https://doi.org/10.1016/j.biomaterials.2014.07.051.

Birkhold, A.I., Razi, H., Duda, G.N., Weinkamer, R., Checa, S., Willie, B.M., 2016. The periosteal bone surface is less mechano-responsive than the endocortical. Sci. Rep. 6 (March), 1–11. https://doi.org/10.1038/srep23480.

Brunkow, M.E., Gardner, J.C., Van Ness, J., Paeper, B.W., Kovacevich, B.R., Proll, S., Skonier, J.E., Zhao, L., Sabo, P.J., Fu, Y.H., Alisch, R.S., Gillett, L., Colbert, T., Tacconi, P., Galas, D., Hamersma, H., Beighton, P., Mulligan, J.T., 2001. Bone dysplasia sclerosteosis results from loss of the SOST gene product, a novel cystine knot-containing protein. Am. J. Hum. Genet. 68 (3), 577–589. https://doi.org/10.1086/318811.

Burr, D.B., Allen, M.R., 2019. Basic and Applied Bone Biology. https://doi.org/10.1016/b978-0-12-813259-3.01001-0.

Carriero, A., Zimmermann, E.A., Paluszny, A., Tang, S.Y., Bale, H., Busse, B., Alliston, T., Kazakia, G., Ritchie, R.O., Shefelbine, S.J., 2014a. How tough is brittle bone? Investigating osteogenesis imperfecta in mouse bone. https://doi.org/10.1002/jbmr.2172.

Carriero, A., Zimmermann, E.A., Shefelbine, S.J., Ritchie, R.O., 2014b. A methodology for the investigation of toughness and crack propagation in mouse bone. J. Mech. Behav. Biomed. Mater. 39, 38–47. https://doi.org/10.1016/J.JMBBM.2014.06.017.

Casanova, M., Schindeler, A., Peacock, L., Lee, L., Schneider, P., Little, D.G., Müller, R., 2021. Characterization of the developing lacunocanalicular network during fracture repair. JBMR Plus 5 (9), 1–9. https://doi.org/10.1002/jbm4.10525.

Catalano, A., Bellone, F., Morabito, N., Corica, F., 2020. Sclerostin and vascular pathophysiology. Int. J. Mol. Sci. 21 (13), 4779. https://doi.org/10.3390/IJMS21134779.

Checa, S., Hesse, B., Roschger, P., Aido, M., Duda, G.N., Raum, K., Willie, B.M., 2015. Skeletal maturation substantially affects elastic tissue properties in the endosteal and periosteal regions of loaded mice tibiae. Acta Biomater. 21, 154–164. https://doi.org/10.1016/j.actbio.2015.04.020.

Compton, J.T., Lee, F.Y., 2014. Current concepts review: a review of osteocyte function and the emerging importance of sclerostin. J. Bone Joint Surg. Am. 96 (19), 1659–1668. https://doi.org/10.2106/JBJS.M.01096.

Currey, J.D., 1988. The effect of porosity and mineral content on the young's modulus of elasticity of compact bone. J. Biomech. 21 (2), 131–139. https://doi.org/10.1016/0021-9290(88)90006-1.

De Maré, A., Opdebeeck, B., Neven, E., D'Haese, P.C., Verhulst, A., 2022. Sclerostin protects against vascular calcification development in mice. J. Bone Miner. Res. 37 (4), 687–699. https://doi.org/10.1002/JBMR.4503.

De Paolis, A., Miller, B.J., Doube, M., Bodey, A.J., Rau, C., Richter, C.P., Cardoso, L., Carriero, A., 2021. Increased cochlear otic capsule thickness and intracortical canal porosity in the oim mouse model of osteogenesis imperfecta. J. Struct. Biol. 213 (2), 107708. https://doi.org/10.1016/J.JSB.2021.107708.

Delgado-Calle, J., Sato, A.Y., Bellido, T., 2016. Role and mechanism of action of sclerostin in bone. Bone 96, 29. https://doi.org/10.1016/j.bone.2016.10.007.

Dreyer, T.J., Keen, J.A., Wells, L.M., Roberts, S.J., 2023. Novel insights on the effect of sclerostin on bone and other organs. J. Endocrinol. 257 (2). https://doi.org/10.1530/JOE-22-0209.

Ferguson, V.L., Ayers, R.A., Bateman, T.A., Simske, S.J., 2003. Bone development and age-related bone loss in male C57BL/6J mice. https://doi.org/10.1016/S8756-3282(03)00199-6.

Ford, S., Tiedemann, K., Shapiro, R., Komarova, S.V., Jähn-Rickert, K., Zimmermann, E. A., 2025. Fluorescent mapping of osteocyte-driven bone formation at pre-osteocyte and mature osteocyte lacunae. Acta Biomater. https://doi.org/10.1016/J.ACTBIO.2025.09.040.

Glatt, V., Canalis, E., Stadmeyer, L., Bouxsein, M.L., 2007. Age-related changes in trabecular architecture differ in female and male C57BL/6J mice. J. Bone Miner. Res. 22 (8), 1197–1207. https://doi.org/10.1359/JBMR.070507.

Glorieux, F.H., Devogelaer, J.P., Durigova, M., Goemaere, S., Hemsley, S., Jakob, F., Junker, U., Ruckle, J., Seefried, L., Winkle, P.J., 2017. BPS804 anti-Sclerostin antibody in adults with moderate osteogenesis imperfecta: results of a randomized phase 2a trial. J. Bone Miner. Res. 32 (7), 1496–1504. https://doi.org/10.1002/JBMR.3143.

Glorieux, F.H., Langdahl, B., Chapurlat, R., De Beur, S.J., Sutton, V.R., Poole, K.E.S., Dahir, K.M., Orwoll, E.S., Willie, B.M., Mikolajewicz, N., Zimmermann, E., Hosseinitabatabaei, S., Ominsky, M.S., Saville, C., Clancy, J., Mackinnon, A., Mistry, A., Javaid, M.K., 2024. Setrusumab for the treatment of osteogenesis imperfecta: 12-month results from the phase 2b asteroid study. J. Bone Miner. Res. 39 (9), 1215–1228. https://doi.org/10.1093/jbmr/zjae112.

Goff, E., Buccino, F., Bregoli, C., McKinley, J.P., Aeppli, B., Recker, R.R., Shane, E., Cohen, A., Kuhn, G., Müller, R., 2021. Large-scale quantification of human osteocyte lacunar morphological biomarkers as assessed by ultra-high-resolution desktop micro-computed tomography. Bone 152. https://doi.org/10.1016/j.bone.2021.116094.

Golledge, J., Thanigaimani, S., 2022. Role of sclerostin in cardiovascular disease. Arterioscler. Thromb. Vasc. Biol. 42 (7), E187–E202. https://doi.org/10.1161/ATVBAHA.122.317635/ASSET/46110263-9606-4123-A9FD-6FF91BE4C776/ASSETS/GRAPHIC/ATVBAHA.122.317635.FIG 05.JPG.

Hemmatian, H., Laurent, M.R., Bakker, A.D., Vanderschueren, D., Klein-Nulend, J., Harry Van Lenthe, G., 2018. Age-related changes in female mouse cortical bone microporosity. https://doi.org/10.1016/j.bone.2018.05.003.

Heveran, C.M., Rauff, A., King, K.B., Carpenter, R.D., Ferguson, V.L., 2018. A new open-source tool for measuring 3D osteocyte lacunar geometries from confocal laser scanning microscopy reveals age-related changes to lacunar size and shape in cortical mouse bone. Bone 110, 115–127. https://doi.org/10.1016/J.BONE.2018.01.018.

Hosseinitabatabaei, S., Vitienes, I., Rummler, M., Birkhold, A., Rauch, F., Willie, B.M., 2025. Non-invasive quantification of bone (re)modeling dynamics in adults with osteogenesis imperfecta treated with setrusumab using timelapse high-resolution peripheral-quantitative computed tomography. J. Bone Miner. Res. 40 (3), 348–361. https://doi.org/10.1093/JBMR/ZJAF013.

Huang, J., Ma, T., Wang, C., Wang, Z., Wang, X., Hua, B., Jiang, C., Yan, Z., 2024. SOST/Sclerostin impairs the osteogenesis and angiogesis in glucocorticoid-associated osteonecrosis of femoral head. Mol. Med. 30 (1), 1–14. https://doi.org/10.1186/S10020-024-00933-5/FIGURES/8.

Kaya, S., Basta-Pljakic, J., Seref-Ferlengez, Z., Majeska, R.J., Cardoso, L., Bromage, T.G., Zhang, Q., Flach, C.R., Mendelsohn, R., Yakar, S., Fritton, S.P., Schaffler, M.B., 2017.

Lactation-induced changes in the volume of osteocyte lacunar-canalicular space alter mechanical properties in cortical bone tissue. J. Bone Miner. Res. 32 (4), 688–697. https://doi.org/10.1002/JBMR.3044;REQUESTEDJOURNAL:JOURNAL:15234681;WGROUP:STRING:PUBLICATION.

Kogawa, M., Wijenayaka, A.R., Ormsby, R.T., Thomas, G.P., Anderson, P.H., Bonewald, L.F., Findlay, D.M., Atkins, G.J., 2013. Sclerostin regulates release of Bone mineral by osteocytes by induction of carbonic anhydrase 2. J. Bone Miner. Res. 28 (12), 2436–2448. https://doi.org/10.1002/JBMR.2003.

Kogawa, M., Khalid, K.A., Wijenayaka, A.R., Ormsby, R.T., Evdokiou, A., Anderson, P.H., Findlay, D.M., Atkins, G.J., 2018. Recombinant sclerostin antagonizes effects of ex vivo mechanical loading in trabecular bone and increases osteocyte lacunar size. Am. J. Physiol. Cell Physiol. 314 (1), C53–C61. https://doi.org/10.1152/ajpcell.00175.2017.

Kruck, B., Zimmermann, E.A., Damerow, S., Figge, C., Julien, C., Wulsten, D., Thiele, T., Martin, M., Hamdy, R., Reumann, M.K., Duda, G.N., Checa, S., Willie, B.M., 2018. Sclerostin neutralizing antibody treatment enhances Bone formation but does not rescue mechanically induced delayed healing. J. Bone Miner. Res. 33 (9), 1686–1697. https://doi.org/10.1002/jbmr.3454.

Langdahl, B.L., Hofbauer, L.C., Forfar, J.C., 2021. Cardiovascular safety and sclerostin inhibition. J. Clin. Endocrinol. Metab. 106 (7), 1845–1853. https://doi.org/10.1210/CLINEM/DGAB193.

Lewiecki, E.M., Blicharski, T., Goemaere, S., Lippuner, K., Meisner, P.D., Miller, P.D., Miyauchi, A., Maddox, J., Chen, L., Horlait, S., 2018. A phase III randomized placebo-controlled trial to evaluate efficacy and safety of Romosozumab in men with osteoporosis. J. Clin. Endocrinol. Metab. 103 (9), 3183–3193. https://doi.org/10.1210/jc.2017-02163.

Li, X., Ominsky, M.S., Niu, Q.T., Sun, N., Daugherty, B., D'Agostin, D., Kurahara, C., Gao, Y., Cao, J., Gong, J., Asuncion, F., Barrero, M., Warmington, K., Dwyer, D., Stolina, M., Morony, S., Sarosi, I., Kostenuik, P.J., Lacey, D.L., Paszty, C., 2008. Targeted deletion of the sclerostin gene in mice results in increased bone formation and bone strength. J. Bone Miner. Res. 23 (6), 860–869. https://doi.org/10.1359/JBMR.080216.

Mader, K.S., Schneider, P., Müller, R., Stampanoni, M., 2013. A quantitative framework for the 3D characterization of the osteocyte lacunar system. Bone 57 (1), 142–154. https://doi.org/10.1016/j.bone.2013.06.026.

Mcclung, M.R., Grauer, A., Boonen, S., Bolognese, M.A., Brown, J.P., Diez-Perez, A., Langdahl, B.L., Reginster, J.-Y., Zanchetta, J.R., Wasserman, S.M., Katz, L., Maddox, J., Yang, Y.-C., Libanati, C., Bone, H.G., 2014. Romosozumab in postmenopausal women with low bone mineral density. N. Engl. J. Med. 370, 412–432. https://doi.org/10.1056/NEJMoa1305224.

Mirone, A., Brun, E., Gouillart, E., Tafforeau, P., Kieffer, J., 2013. PyHST2: an hybrid distributed code for high speed tomographic reconstruction with iterative reconstruction and a priori knowledge capabilities. Nucl. Instrum. Methods Phys. Res., Sect. B 324, 41–48. https://doi.org/10.1016/j.nimb.2013.09.030.

Moharrer, Y., Boerckel, J.D., 2021. Tunnels in the rock: dynamics of osteocyte morphogenesis. Bone 153, 116104. https://doi.org/10.1016/J.BONE.2021.116104.

Mosey, H., Núñez, J.A., Goring, A., Clarkin, C.E., Staines, K.A., Lee, P.D., Pitsillides, A.A., Javaheri, B., 2017. Sost deficiency does not alter bone's lacunar or vascular porosity in mice. Front. Mater. 4 (September). https://doi.org/10.3389/fmats.2017.00027.

Muñoz, A., De Paolis, A., Cardoso, L., Carriero, A., 2025a. Mechanical deformations of bone generate interstitial fluid flow at nanoscale velocities around osteocytes. Front. Bioeng. Biotechnol. 13, 1639788. https://doi.org/10.3389/FBIOE.2025.1639788/BIBTEX.

Muñoz, A., De Paolis, A., Cardoso, L., Carriero, A., 2025b. Osteocyte-lacuna shape and canaliculi architecture dictate fluid flow around osteocyte, and strain of cell and bone matrix: implications for cell mechanobiology and bone fragility. Bone 200, 117613. https://doi.org/10.1016/J.BONE.2025.117613.

Nicolella, D.P., Moravits, D.E., Gale, A.M., Bonewald, L.F., Lankford, J., 2005. Osteocyte lacunae tissue strain in cortical bone. J. Biomech. 39 (9), 1735. https://doi.org/10.1016/J.JBIOMECH.2005.04.032.

Núñez, J.A., Goring, A., Hesse, E., Thurner, P.J., Schneider, P., Clarkin, C.E., 2017. Simultaneous visualisation of calcified bone microstructure and intracortical vasculature using synchrotron X-ray phase contrast-enhanced tomography. Sci. Rep. 7 (1), 13289. https://doi.org/10.1038/s41598-017-13632-5.

Olsen, J.J., Pohl, S. öther G., Deshmukh, A., Visweswaran, M., Ward, N.C., Arfuso, F., Agostino, M., Dharmarajan, A., 2017. The role of Wnt signalling in angiogenesis. Clin. Biochem. Rev. 38 (3), 131. https://pmc.ncbi.nlm.nih.gov/articles/PMC5759160/.

Oranger, A., Brunetti, G., Colaianni, G., Tamma, R., Carbone, C., Lippo, L., Mori, G., Pignataro, P., Cirulli, N., Zerlotin, R., Moretti, B., Notarnicola, A., Ribatti, D., Grano, M., Colucci, S., 2017. Sclerostin stimulates angiogenesis in human endothelial cells. Bone 101, 26–36. https://doi.org/10.1016/J.BONE.2017.03.001.

Piemontese, M., Almeida, M., Robling, A.G., Kim, H.N., Xiong, J., Thostenson, J.D., Weinstein, R.S., Manolagas, S.C., O'Brien, C.A., Jilka, R.L., 2017. Old age causes de novo intracortical bone remodeling and porosity in mice. JCI Insight 2 (17), e93771. https://doi.org/10.1172/JCI.INSIGHT.93771.

Prideaux, M., Findlay, D.M., Atkins, G.J., 2016. Osteocytes: the master cells in bone remodelling. Curr. Opin. Pharmacol. 28, 24–30. https://doi.org/10.1016/J.COPH.2016.02.003.

Qin, W., Li, X., Peng, Y., Harlow, L.M., Ren, Y., Wu, Y., Li, J., Qin, Y., Sun, J., Zheng, S., Brown, T., Feng, J.Q., Ke, H.Z., Bauman, W.A., Cardozo, C.C., 2015. Sclerostin antibody preserves the morphology and structure of osteocytes and blocks the severe skeletal deterioration after motor-complete spinal cord injury in rats. J. Bone Miner. Res. 30 (11), 1994–2004. https://doi.org/10.1002/JBMR.2549.

Qing, H., Ardeshirpour, L., Divieti Pajevic, P., Dusevich, V., Jähn, K., Kato, S., Wysolmerski, J., Bonewald, L.F., 2012. Demonstration of osteocytic perilacunar/canalicular remodeling in mice during lactation. J. Bone Miner. Res. 27 (5), 1018–1029. https://doi.org/10.1002/JBMR.1567.

Roudier, M., Li, X., Niu, Q.T., Pacheco, E., Pretorius, J.K., Graham, K., Yoon, B.R.P., Gong, J., Warmington, K., Ke, H.Z., Black, R.A., Hulme, J., Babij, P., 2013. Sclerostin is expressed in articular cartilage but loss or inhibition does not affect cartilage remodeling during aging or following mechanical injury. Arthritis Rheum. 65 (3), 721–731. https://doi.org/10.1002/ART.37802.

Rummler, M., Schemenz, V., McCluskey, S., Davydok, A., Rauch, F., Glorieux, F.H., Harrington, M.J., Wagermaier, W., Willie, B.M., Zimmermann, E.A., 2024. Bone matrix properties in adults with osteogenesis imperfecta are not adversely affected by setrusumab—a sclerostin neutralizing antibody. J. Bone Miner. Res. 39 (9), 1229–1239. https://doi.org/10.1093/jbmr/zjae108.

Saag, K.G., Petersen, J., Brandi, M.L., Karaplis, A.C., Lorentzon, M., Thomas, T., Maddox, J., Fan, M., Meisner, P.D., Grauer, A., 2017. Romosozumab or alendronate for fracture prevention in women with osteoporosis. N. Engl. J. Med. 377 (15), 1417–1427. https://doi.org/10.1056/NEJMOA1708322/SUPPL_FILE/NEJMOA1708322_DISCLOSURES.PDF.

Sarahrudi, K., Thomas, A., Albrecht, C., Aharinejad, S., 2012. Strongly enhanced levels of sclerostin during human fracture healing. J. Orthop. Res. 30 (10), 1549–1555. https://doi.org/10.1002/jor.22129.

Schaffler, M.B., Burr, D.B., 1988. Stiffness of compact bone: effects of porosity and density. J. Biomech. 21 (1), 13–16. https://doi.org/10.1016/0021-9290(88)90186-8.

Schemenz, V., Gjardy, A., Chamasemani, F.F., Roschger, A., Roschger, P., Zaslansky, P., Helfen, L., Burghammer, M., Fratzl, P., Weinkamer, R., Brunner, R., Willie, B.M., Wagermaier, W., 2020. Heterogeneity of the osteocyte lacuno-canalicular network architecture and material characteristics across different tissue types in healing bone. J. Struct. Biol. 212 (2), 107616. https://doi.org/10.1016/j.jsb.2020.107616.

Schemitsch, E.H., Miclau, T., Karachalios, T., Nowak, L.L., Sancheti, P., Poolman, R.W., Caminis, J., Daizadeh, N., Dent-Acosta, R.E., Egbuna, O., Chines, A., Maddox, J., Grauer, A., Bhandari, M., 2020. A randomized, placebo-controlled study of Romosozumab for the treatment of hip fractures. J. Bone Joint Surg. Am. Vol. 102 (8), 693–702. https://doi.org/10.2106/JBJS.19.00790.

Shipov, A., Zaslansky, P., Riesemeier, H., Segev, G., Atkins, A., Shahar, R., 2013. Unremodeled endochondral bone is a major architectural component of the cortical bone of the rat (Rattus norvegicus). J. Struct. Biol. 183 (2), 132–140. https://doi.org/10.1016/J.JSB.2013.04.010.

Tiede-Lewis, L.A.M., Dallas, S.L., 2019. Changes in the osteocyte lacunocanalicular network with aging. Bone 122 (January), 101–113. https://doi.org/10.1016/j.bone.2019.01.025.

Tiede-Lewis, L.A.M., Xie, Y., Hulbert, M.A., Campos, R., Dallas, M.R., Dusevich, V., Bonewald, L.F., Dallas, S.L., 2017. Degeneration of the osteocyte network in the C57BL/6 mouse model of aging. Aging 9 (10), 2190–2208. https://doi.org/10.18632/AGING.101308.

Ugarteburu, M., Doube, M., Witek, L., Rau, C., Cardoso, L., Richter, C.P., Carriero, A., 2025. Small and porous ossicles, with flat stapes footplate and incudal fractures in the oim mouse model of osteogenesis imperfecta. Bone 196, 117495. https://doi.org/10.1016/J.BONE.2025.117495.

Virk, M.S., Alaee, F., Tang, H., Ominsky, M.S., Ke, H.Z., Lieberman, J.R., 2013. Systemic administration of sclerostin antibody enhances bone repair in a critical-sized femoral defect in a rat model. J. Bone Joint Surg. 95 (8), 694–701. https://doi.org/10.2106/JBJS.L.00285.

Wagermaier, W., Klaushofer, K., Fratzl, P., 2015. Fragility of Bone material controlled by internal interfaces. Calcif. Tissue Int. 97 (3), 201–212. https://doi.org/10.1007/s00223-015-9978-4.

Wang, J.S., Kamath, T., Mazur, C.M., Mirzamohammadi, F., Rotter, D., Hojo, H., Castro, C.D., Tokavanich, N., Patel, R., Govea, N., Enishi, T., Wu, Y., da Silva Martins, J., Bruce, M., Brooks, D.J., Bouxsein, M.L., Tokarz, D., Lin, C.P., Abdul, A., Wein, M.N., 2021. Control of osteocyte dendrite formation by Sp7 and its target gene osteocrin. Nat. Commun. 12 (1), 6271. https://doi.org/10.1038/s41467-021-26571-7.

Wijenayaka, A.R., Kogawa, M., Lim, H.P., Bonewald, L.F., Findlay, D.M., Atkins, G.J., 2011. Sclerostin stimulates osteocyte support of osteoclast activity by a RANKL-dependent pathway. PLoS One 6 (10), e25900. https://doi.org/10.1371/JOURNAL.PONE.0025900.

Willie, B.M., Birkhold, A.I., Razi, H., Thiele, T., Aido, M., Kruck, B., Schill, A., Checa, S., Main, R.P., Duda, G.N., 2013. Diminished response to in vivo mechanical loading in trabecular and not cortical bone in adulthood of female C57Bl/6 mice coincides with a reduction in deformation to load. Bone 55 (2), 335–346. https://doi.org/10.1016/j.bone.2013.04.023.